Physics Letters B 806 (2020) 135486

Contents lists available at ScienceDirect

Physics Letters B

www.elsevier.com/locate/physletb

Υ production in p–Pb collisions at $\sqrt{s_{\rm NN}} = 8.16$ TeV

ALICE Collaboration [⋆]

ARTICLE INFO

Article history:
Received 16 November 2019
Received in revised form 29 April 2020
Accepted 11 May 2020
Available online 20 May 2020
Editor: D.F. Geesaman

ABSTRACT

Υ production in p–Pb interactions is studied at the centre-of-mass energy per nucleon–nucleon collision $\sqrt{s_{\rm NN}} = 8.16$ TeV with the ALICE detector at the CERN LHC. The measurement is performed reconstructing bottomonium resonances via their dimuon decay channel, in the centre-of-mass rapidity intervals $2.03 < y_{\rm cms} < 3.53$ and $-4.46 < y_{\rm cms} < -2.96$, down to zero transverse momentum. In this work, results on the Υ(1S) production cross section as a function of rapidity and transverse momentum are presented. The corresponding nuclear modification factor shows a suppression of the Υ(1S) yields with respect to pp collisions, both at forward and backward rapidity. This suppression is stronger in the low transverse momentum region and shows no significant dependence on the centrality of the interactions. Furthermore, the Υ(2S) nuclear modification factor is evaluated, suggesting a suppression similar to that of the Υ(1S). A first measurement of the Υ(3S) has also been performed. Finally, results are compared with previous ALICE measurements in p–Pb collisions at $\sqrt{s_{\rm NN}} = 5.02$ TeV and with theoretical calculations.

1. Introduction

Quarkonium resonances, i.e. bound states of a heavy quark (Q) and anti-quark ($\overline{\rm Q}$), are well-known probes of the formation of a quark–gluon plasma (QGP) which can occur in heavy-ions collisions. The high colour-charge density reached in such a medium can, in fact, screen the binding force between the Q and $\overline{\rm Q}$, leading to a temperature-dependent melting of the quarkonium states according to their binding energies [1].

A suppression of bottomonium resonances, the bound states formed by b and $\overline{\rm b}$ quarks, was observed in Pb–Pb collisions, at the LHC energies of $\sqrt{s_{\rm NN}} = 2.76$ TeV and $\sqrt{s_{\rm NN}} = 5.02$ TeV by the ALICE [2,3] and CMS [4–6] experiments. All the Υ resonances show a reduction in their production yields compared to pp interactions at the same centre-of-mass energy, scaled by the number of nucleon–nucleon collisions. Furthermore, the magnitude of the suppression is significantly different for the three resonances and it increases from the tightly bound Υ(1S) to the loosely bound Υ(3S) [4–6], as expected in a sequential suppression scenario, with the binding energies of the Υ states ranging between ∼1 GeV for the Υ(1S) to ∼0.2 GeV for the Υ(3S) [7]. Modifications to the bottomonium production might also be induced by cold nuclear matter (CNM) mechanisms not related to the formation of the QGP. The modification of the quark and gluon structure functions for nucleons inside nuclei, modelled either via nuclear parton distribution functions (nPDFs) [8–11] or through a Color Glass Condensate effective theory [12], or the coherent energy loss of the $\rm Q\overline{Q}$ pair during its path through the cold nuclear medium [13] are examples of CNM effects which can influence quarkonium production [14]. The size of these effects is usually assessed in proton–nucleus collisions. These interactions also allow for the investigation of additional final state mechanisms, which can modify the production in particular of the more loosely bound resonances [15–17].

ALICE has published results on the modification of the Υ(1S) production yields as a function of the centre-of-mass rapidity ($y_{\rm cms}$) using the 2013 p–Pb collisions data sample at $\sqrt{s_{\rm NN}} = 5.02$ TeV [18]. The size of the observed suppression was found to be similar in the forward and backward rapidity regions. Theoretical calculations based on the aforementioned CNM mechanisms fairly describe the forward-$y_{\rm cms}$ measurements, while they slightly overestimate the results obtained at backward rapidity. Furthermore, the measurement of the Υ(2S) to Υ(1S) ratio [18], Υ(2S)/Υ(1S), was consistent, albeit within large uncertainties, with the one obtained in pp collisions [19], suggesting CNM effects of the same size on the two resonances both at forward and backward rapidity. Consistent results were also obtained by the LHCb experiment [20] in a similar kinematic region. However, it should be noted that ATLAS [21] and CMS [22] measurements of Υ(2S)/Υ(1S) at midrapidity suggest a stronger suppression of the Υ(2S) with respect to the Υ(1S) state, as expected if final state effects are at play [15].

In 2016, the LHC delivered p–Pb collisions at $\sqrt{s_{\rm NN}} = 8.16$ TeV. The increase both in integrated luminosity, about a factor of 2

[⋆] *E-mail address:* alice-publications@cern.ch.

https://doi.org/10.1016/j.physletb.2020.135486

larger than the one collected in 2013, and in the bottomonium production cross section, due to the higher centre-of-mass energy, allows a more detailed study of the production of the Υ states. In this paper, results on the $\Upsilon(1S)$ production as a function of $y_{\rm cms}$, transverse momentum ($p_{\rm T}$) and centrality of the collisions will be discussed and compared with the measurements performed in p–Pb collisions at $\sqrt{s_{\rm NN}} = 5.02$ TeV and with theoretical calculations. A comparison of the $\Upsilon(2S)$ and $\Upsilon(3S)$ to $\Upsilon(1S)$ production yields and nuclear modification factors, integrated over $y_{\rm cms}$, $p_{\rm T}$ and centrality, will also be presented. Finally, the results will be compared with the corresponding measurements obtained by LHCb at the same energy [23]. It should be noted that all the presented results refer to the Υ inclusive production, i.e. to Υ either produced directly or coming from the feed-down of higher-mass excited states.

2. Experimental apparatus and data sample

A detailed description of the ALICE apparatus and performance can be found in [24,25]. The forward muon spectrometer [26] is the main detector used in this analysis. It consists of five tracking stations made of two planes of Cathode Pad Chambers each, followed by two trigger stations each one composed by two planes of Resistive Plate Chambers. A 10 interaction-length ($\lambda_{\rm I}$) absorber, placed in front of the tracking system, filters out most of the hadrons produced in the collisions. Low-momentum muons and hadrons escaping the first absorber are stopped by a second 7.2 $\lambda_{\rm I}$-thick iron wall, placed in front of the trigger stations. The momentum of the particles is evaluated by measuring their curvature in a dipole magnet with a 3 T×m integrated field. The muon spectrometer measures muons in the pseudorapidity interval $-4 < \eta < -2.5$ in the laboratory reference frame. It also provides single and unlike- or like-sign dimuon triggers based on the detection in the trigger system of one or two muons, respectively, having a transverse momentum higher than a programmable threshold set to $p_{\rm T,\mu} = 0.5$ GeV/c. This threshold is not sharp and the single muon trigger efficiency reaches a plateau value of $\sim$98% at about $p_{\rm T,\mu} \sim 1.5$ GeV/c.

The primary interaction vertex of the collision is reconstructed using the two innermost layers of the Inner Tracking System (Silicon Pixel Detector, SPD) [27], extending over the pseudorapidity intervals $|\eta| < 2$ and $|\eta| < 1.4$, respectively. The V0 detector [28], composed of two sets of scintillators covering the pseudorapidity intervals $2.8 < \eta < 5.1$ and $-3.7 < \eta < -1.7$, provides the luminosity measurement, which can also be obtained independently from the information of the T0 Cherenkov detectors [29], covering the regions $4.6 < \eta < 4.9$ and $-3.3 < \eta < -3$. The V0 detector is also used to provide the minimum bias (MB) trigger, defined by the coincidence of signals in the two sets of scintillators. The trigger condition used in this analysis is based on the coincidence of the MB trigger with the unlike-sign dimuon one ($\mu\mu$-MB). The removal of beam-induced background is based on the timing information provided by the V0 and by two sets of Zero Degree Calorimeters (ZDC) [30] placed at ±112.5 m from the interaction point, along the beamline. The ZDCs are also used for the centrality estimation as it will be discussed in Sec. 3. Finally, for the study of the Υ production as a function of the centrality of the collisions, pile-up events in which two or more interactions occur in the same colliding bunch are removed using the information from SPD and V0.

Further selection criteria, commonly adopted in the ALICE quarkonium analyses (see e.g. [18,31]), are applied to the muon tracks forming the dimuon pair. Muon tracks must have a pseudorapidity value in the range $-4 < \eta_\mu < -2.5$, corresponding to the muon spectrometer acceptance, and they should point to the interaction vertex to remove fake tracks and particles not directly produced in beam–beam interactions. Their transverse coordinate at the end of the front absorber ($R_{\rm abs}$) must be within 17.6 cm $< R_{\rm abs} <$ 89.5 cm, to remove muons not passing the homogeneous region of the absorber. Finally, tracks reconstructed in the tracking chambers of the muon spectrometer should match the track segments reconstructed in the trigger system. This matching request helps to further reject hadron contamination and ensures that the reconstructed muons fulfill the trigger condition.

The data were collected with two beam configurations obtained by inverting the directions of the proton and Pb beams circulating inside the LHC. In this way it was possible to cover both a forward ($2.03 < y_{\rm cms} < 3.53$) and a backward ($-4.46 < y_{\rm cms} < -2.96$) dimuon rapidity interval, where the positive (negative) $y_{\rm cms}$ refers to the proton (Pb) beam going towards the muon spectrometer. The collected integrated luminosities for the corresponding data samples, referred to as p–Pb (forward rapidity) and Pb–p (backward rapidity) in the following, are $\mathscr{L}_{\rm int}^{\rm pPb} = 8.4 \pm 0.2$ nb^{-1} and $\mathscr{L}_{\rm int}^{\rm Pbp} = 12.8 \pm 0.3$ nb^{-1} [32].

3. Data analysis

The results presented in this paper are based on an analysis procedure similar to the one described in [18] for the study of the Υ production in p–Pb collisions at $\sqrt{s_{\rm NN}} = 5.02$ TeV.

The $\Upsilon(1S)$, $\Upsilon(2S)$ and $\Upsilon(3S)$ production cross sections, corrected by the branching ratio for the decay in a muon pair (B.R.$_{\Upsilon\to\mu^+\mu^-}$), are obtained, for a given ($\Delta y_{\rm cms}$, $\Delta p_{\rm T}$) interval, as

$$\frac{{\rm d}^2\sigma_{\rm pPb}^{\Upsilon}}{{\rm d}y_{\rm cms}{\rm d}p_{\rm T}} = \frac{N_\Upsilon}{\mathscr{L}_{\rm int}^{\rm pPb} \times (A\times\varepsilon) \times \Delta y_{\rm cms} \times \Delta p_{\rm T} \times {\rm B.R.}_{\Upsilon\to\mu^+\mu^-}}, \tag{1}$$

where N_Υ is the number of signal counts and $(A\times\varepsilon)$ is the corresponding acceptance and efficiency correction in the kinematic bin under study, while the branching ratios are (2.48 ± 0.05)% for $\Upsilon(1S)$, (1.93 ± 0.17)% for $\Upsilon(2S)$ and (2.18 ± 0.21)% for $\Upsilon(3S)$ [33].

The number of $\Upsilon(nS)$ is obtained by fitting the unlike-sign dimuon invariant mass spectrum with a combination of signal shapes to describe the Υ resonances and an empirical function to model the background. More in detail, the background is described by several combinations of exponential and polynomial functions or by a Gaussian function with a mass-dependent width. For the resonance shapes, extended Crystal Ball functions [34], with power-law tails on the right and left sides of the mass peak are used. Alternatively, pseudo-Gaussian functions with a mass-dependent width are also adopted [34]. The same signal shape is chosen for all the Υ states. The mass of the $\Upsilon(1S)$ and its width $\sigma_{\Upsilon(1S)}$ are free parameters of the fit, while the mass and the width of the $\Upsilon(2S)$ and $\Upsilon(3S)$ states are bound to those of the $\Upsilon(1S)$ in the following way: $m_{\Upsilon(nS)} = m_{\Upsilon(1S)} + (m^{\rm PDG}_{\Upsilon(nS)} - m^{\rm PDG}_{\Upsilon(1S)})$ and $\sigma_{\Upsilon(nS)} = \sigma_{\Upsilon(1S)} \times \sigma^{\rm MC}_{\Upsilon(nS)}/\sigma^{\rm MC}_{\Upsilon(1S)}$. The mass value $m^{\rm PDG}_{\Upsilon(nS)}$ is taken from [33] and $\sigma^{\rm MC}_{\Upsilon(nS)}$ is the width of the resonance as evaluated from a fit, with the aforementioned signal functions, to the spectrum obtained from the Monte Carlo (MC) simulation also used for the $(A\times\varepsilon)$ correction. Due to the signal-over-background ratio of the order of $\sim$0.7 ($\sim$1) in p–Pb (Pb–p), measured in a 3σ region around the $\Upsilon(1S)$ mass, the non-Gaussian tails of the extended Crystal Ball function can not be kept as free parameters of the fits. Hence, they are tuned on pp data at $\sqrt{s} = 13$ TeV, the largest data sample collected by ALICE so far, or, alternatively, on p–Pb or pp MC simulations at $\sqrt{s_{\rm NN}} = 8.16$ TeV and $\sqrt{s} = 8$ TeV, respectively. The same tails are adopted for the $\Upsilon(2S)$ and $\Upsilon(3S)$ mass shapes. Examples of the fit to the invariant mass spectrum, for both the p–Pb and Pb–p samples, are shown in Fig. 1.

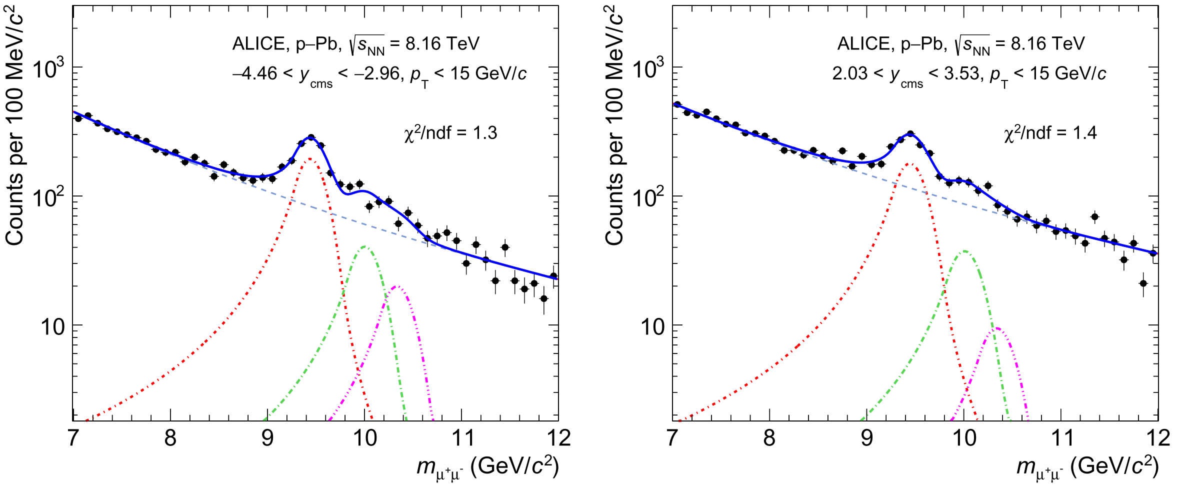

Fig. 1. Invariant mass spectra of unlike-sign dimuons, integrated over p_T, for Pb–p (left panel) and p–Pb (right panel) collisions. The shapes of the $\Upsilon(1S)$, $\Upsilon(2S)$ and $\Upsilon(3S)$ resonances are shown (dash-dotted lines), together with the background function (dashed line) and the total fit (solid line).

The number of Υ candidates, N_Υ, is evaluated as the average of the values obtained by varying the signal and background functions as well as the fitting intervals (6 GeV/c^2 $< m_{\mu\mu} <$ 13 GeV/c^2 or 7 GeV/c^2 $< m_{\mu\mu} <$ 12 GeV/c^2). The statistical uncertainties are calculated as the average of the statistical uncertainties over the various fits and the standard deviation of the distribution of the N_Υ values provides the systematic uncertainties on the signal extraction. For the $\Upsilon(2S)$ and $\Upsilon(3S)$ cases, an additional contribution to the systematic uncertainty is included, to account for possible variations of their width with respect to that of the $\Upsilon(1S)$. In particular, their widths are allowed to vary between a minimum value $\sigma_{\Upsilon(1S)}$ and a maximum value $\sigma_{\Upsilon(1S)} \times \sigma^{MC}_{\Upsilon(nS)}/\sigma^{MC}_{\Upsilon(1S)}$, where the ratio $\sigma^{MC}_{\Upsilon(nS)}/\sigma^{MC}_{\Upsilon(1S)}$ is obtained from MC simulations alternative to the ones used for the $(A \times \varepsilon)$ correction, i.e. based on different Υ kinematic input shapes, as it will be discussed later on. A further 5% systematic uncertainty is also included to account for possible residual discrepancies between the detector resolution in MC and in the data.

The total number of $\Upsilon(1S)$, integrated over the full kinematic range, amounts to $N_{\Upsilon(1S)} = 909 \pm 62\,(\text{stat.}) \pm 58\,(\text{syst.})$ and $N_{\Upsilon(1S)} = 918 \pm 55\,(\text{stat.}) \pm 51\,(\text{syst.})$ for the forward and backward-rapidity regions, respectively. Corresponding values for $\Upsilon(2S)$ are $N_{\Upsilon(2S)} = 192 \pm 39\,(\text{stat.}) \pm 17\,(\text{syst.})$ and $N_{\Upsilon(2S)} = 194 \pm 34\,(\text{stat.}) \pm 16\,(\text{syst.})$, while for the $\Upsilon(3S)$ the values are $N_{\Upsilon(3S)} = 48 \pm 36\,(\text{stat.}) \pm 8\,(\text{syst.})$ and $N_{\Upsilon(3S)} = 95 \pm 30\,(\text{stat.}) \pm 12\,(\text{syst.})$. The systematic uncertainty, amounting to $\sim$6% for the $\Upsilon(1S)$ and $\sim$8% for the $\Upsilon(2S)$, is dominated by the choice of the tail parameters in the fit functions and, in the $\Upsilon(2S)$ case, also by the allowed range of variation for the $\sigma_{\Upsilon(2S)}$. In the $\Upsilon(3S)$ case, the systematic uncertainties are slightly larger, amounting to $\sim$17% at forward rapidity and $\sim$12% at backward rapidity. For p_T- or y_{cms}-differential $\Upsilon(1S)$ studies, the systematic uncertainties have a similar size, reaching $\sim$15% only in the highest p_T bin (8 GeV/c $< p_T <$ 15 GeV/c).

The acceptance and efficiency correction is calculated in a MC simulation, based on the GEANT3 transport code [35]. The MC simulation is performed on a run-by-run basis to closely follow the evolution of the performance of the detectors during the data taking. The $\Upsilon(1S)$ are generated using rapidity and transverse momentum distributions tuned on p–Pb or Pb–p data at $\sqrt{s_{NN}} =$ 8.16 TeV, through an iterative procedure [31]. The p_T and y_{cms} integrated $(A \times \varepsilon)$ amounts to 0.300 ± 0.006 for the $\Upsilon(1S)$ at forward rapidity and 0.273 ± 0.007 at backward rapidity, where the quoted uncertainties are systematic, the statistical uncertainties being negligible. The lower $(A \times \varepsilon)$ values measured in the Pb–p period, with respect to the p–Pb one, are due to detector instabilities which affected temporarily the behaviour of two tracking chambers. The limited size of the data sample do not allow for a similar tuning of the p_T and y_{cms} distributions on data for the $\Upsilon(2S)$ and $\Upsilon(3S)$ resonances, hence the same shapes as for the $\Upsilon(1S)$ are used. The resulting $(A \times \varepsilon)$ values show a negligible difference with respect to the $\Upsilon(1S)$ ones. The systematic uncertainties on $(A \times \varepsilon)$ include contributions related to the choice of the MC p_T and y_{cms} input distributions for the Υ states and to the evaluation of the tracking and trigger efficiencies. The systematic uncertainties associated to the MC Υ input shapes are evaluated as the maximum difference between the $(A \times \varepsilon)$ evaluated with the aforementioned MC tuned on data and the values extracted from alternative MC samples based on p_T and y_{cms} Υ distributions either measured by the LHCb experiment in pp collisions at $\sqrt{s} = 8$ TeV [36] or obtained from existing CDF and LHC pp measurements [37–39] via a procedure similar to the one described in [40]. Nuclear shadowing is also included to account for its influence on the bottomonium kinematic distributions. These systematic uncertainties for the three resonances vary between 1% and 1.8%. They have a negligible p_T-dependence, while they reach up to 4% at the edges of the rapidity intervals. The systematic uncertainty on the trigger efficiency consists of two contributions, one related to the evaluation of the intrinsic efficiency of each muon-trigger chamber (1%) and one to small differences between the trigger response function estimated via data and MC (0.6% in p–Pb and 0.2% in Pb–p, when integrating over y_{cms} and p_T). This last source of uncertainty is below 1% also for the p_T or y_{cms}-differential studies. The systematic uncertainty associated to the tracking efficiency is evaluated comparing the dimuon tracking efficiencies computed both in data and MC. These efficiencies are computed combining the efficiency of each single muon-tracking chamber, obtained relying on the redundancy of the tracking system. The resulting systematic uncertainties amount to 1% for p–Pb and 2% for Pb–p, for both the y_{cms} and p_T differential studies and for results integrated over the kinematic domain. Finally, an additional 1% systematic uncertainty on the choice of the χ^2 cut on the matching between the tracks reconstructed in the tracking and in the trigger systems is included. The systematic uncertainties associated to the trigger, tracking and matching efficiencies are considered to be identical for both the $\Upsilon(1S)$ and $\Upsilon(2S)$ resonances.

The integrated luminosities are obtained as $\mathscr{L}_{int} = N_{MB}/\sigma_{MB}$. The number of equivalent minimum bias events, N_{MB}, is evaluated by multiplying the number of events collected with the $\mu\mu$-MB trigger by a factor $F_{\rm norm}$, corresponding to the inverse of the probability of having a triggered dimuon in a MB event [31]. This quantity is computed, run by run, as the ratio between the number of collected MB triggers and the number of times the dimuon trigger condition is verified in the MB trigger sample. Once averaged over all the runs, considering as weight the number of $\mu\mu$-MB triggers in each run, $F_{\rm norm}$ amounts to 679 ± 7 at forward rapidity and 372 ± 4 at backward rapidity. The quoted uncertainty (1%) is systematic and accounts for differences coming from an alternative evaluation method, based on the information provided by the level-0 trigger scalers, as detailed in [41]. The V0-based MB cross section ($\sigma_{\rm MB}$) is measured from a van der Meer scan, and it amounts to 2.09 ± 0.04 b for the p–Pb configuration and 2.10 ± 0.04 b for the Pb–p one [32]. In the luminosity systematic uncertainty quoted in Table 1, the uncertainties on $F_{\rm norm}$ and $\sigma_{\rm MB}$ are combined, together with a 1.1% (0.6%) contribution due to the difference between the luminosities obtained with the V0 and T0 detectors in the p–Pb (Pb–p) configurations [32].

The nuclear effects on the Υ production are studied comparing the corresponding p–Pb production cross section to the one measured in pp collisions, ${\rm d}^2\sigma^{\Upsilon}_{\rm pp}/{\rm d}y_{\rm cms}{\rm d}p_{\rm T}$, obtained at the same centre-of-mass energy and scaled by the atomic mass number of the Pb nucleus ($A_{\rm Pb} = 208$), through the so-called nuclear modification factor $R_{\rm pPb}$, defined as

$$R_{\rm pPb} = \frac{{\rm d}^2\sigma^{\Upsilon}_{\rm pPb}/{\rm d}y_{\rm cms}{\rm d}p_{\rm T}}{A_{\rm Pb} \times {\rm d}^2\sigma^{\Upsilon}_{\rm pp}/{\rm d}y_{\rm cms}{\rm d}p_{\rm T}}. \qquad (2)$$

The proton–proton reference is based on the LHCb measurements of the bottomonium production cross section in pp collisions at $\sqrt{s} = 8$ TeV [36], in $-4.5 < y_{\rm cms} < -2.5$ and $2 < y_{\rm cms} < 4$, corrected by a factor to account for the slightly different centre-of-mass energies of the interactions. This correction factor is evaluated interpolating the LHCb measurements at $\sqrt{s} =$ 7, 8 and 13 TeV [36,42], as detailed in [43]. It amounts to 1.02 for both the Υ(1S) and Υ(2S), showing a negligible $y_{\rm cms}$ dependence and varying by 1% from low to high $p_{\rm T}$. A systematic uncertainty on the determination of this factor (1%) is assigned, based on the choice of the different functions used for the energy-interpolation. The Υ production cross sections in pp collisions at $\sqrt{s}$ = 8 TeV are also measured by ALICE [44]. The results show good agreement with the corresponding LHCb values, but unlike the LHCb measurements, they cover a slightly narrower rapidity region, $2.5 < y_{\rm cms} < 4$, which does not match the rapidity coverage of the p–Pb measurements. The $\sigma^{\Upsilon(1S)}_{\rm pp}$ cross sections, integrated over $p_{\rm T}$ and $y_{\rm cms}$, are 98.5 ± 0.1 (stat.) ± 3.4 (syst.) nb in the range $2.03 < y_{\rm cms} < 3.53$ and 62.0 ± 0.1 (stat.) ± 2.1 (syst.) nb in the range $-4.46 < y_{\rm cms} < -2.96$. The corresponding cross sections for the Υ(2S) are about a factor 3 smaller, being $\sigma^{\Upsilon(2S)}_{\rm pp} = 31.9 \pm 0.1$ (stat.) ± 2.9 (syst.) nb at forward rapidity and 19.7 ± 0.05 (stat.) ± 1.8 (syst.) nb at backward rapidity. The Υ(3S) production cross sections are $\sigma^{\Upsilon(3S)}_{\rm pp} = 12.9 \pm 0.1$ (stat.) ± 1.3 (syst.) nb at forward rapidity and 8.3 ± 0.1 (stat.) ± 0.8 (syst.) nb at backward rapidity.

The large data sample collected in p–Pb collisions in 2016 allows the Υ(1S) production also to be studied as a function of the collision centrality. The centrality determination is based on a hybrid model, as discussed in detail in [45]. In this approach, the centrality is determined by measuring the energy released in the ZDC positioned in the Pb-going direction. For each ZDC-selected centrality class, the average number of collisions $\langle N_{\rm coll}\rangle$ is obtained as $\langle N_{\rm coll}\rangle = \langle N_{\rm part}\rangle$-1, assuming the charged particle multiplicity measured at midrapidity is proportional to the number of participant nucleons, $N_{\rm part}$. The centrality classes used in this analysis correspond to 2–20%, 20–40%, 40–60% and 60–90% of the MB cross section. The 0–2% most central collisions are excluded from this analysis because the fraction of events coming from pile-up in the ZDC is large in this centrality interval and a residual contamination might still be present in spite of the applied pile-up rejection cuts [46].

For centrality studies, the modification induced by the nuclear matter on the Υ(1S) production is quantified through the nuclear modification factor denoted by $Q_{\rm pPb}$, to be distinguished from $R_{\rm pPb}$ since potential biases from the centrality estimation, unrelated to nuclear effects, might be present [45]. The $Q_{\rm pPb}$ is defined as

$$Q_{\rm pPb} = \frac{N_{\Upsilon}}{{\rm B.R.}_{\Upsilon\to\mu^+\mu^-} \times N_{\rm MB} \times (A \times \varepsilon) \times \langle T_{\rm pPb}\rangle \times \sigma^{\Upsilon}_{\rm pp}}. \qquad (3)$$

The quantities entering Eq. (3) are evaluated according to the previously discussed procedure, with few minor differences. When extracting the Υ(1S) signal, for example, no significant variation of the Υ(1S) width as a function of the collision centrality is foreseen. Hence for centrality studies, the Υ(1S) width is fixed to the value obtained in the fit to the centrality-integrated invariant mass spectrum. The uncertainty associated to the choice of the width is accounted for in the evaluation of the systematic uncertainty on the signal extraction. No significant centrality dependence is expected for the $(A \times \varepsilon)$ either, so the centrality-integrated values are also used for all the centrality classes. To evaluate the number of MB events in each centrality class i, $F^{i}_{\rm norm}$ is obtained from the centrality-integrated quantity scaled by the ratio of the number of minimum bias and dimuon-triggered events in each centrality interval with respect to the corresponding centrality integrated quantities, $(N^{i}_{\rm MB}/N_{\rm MB})/(N^{i}_{\mu\mu-{\rm MB}}/N_{\mu\mu-{\rm MB}})$. Alternatively, $F^{i}_{\rm norm}$ is computed directly for each centrality class and a further 1% difference between the two approaches is included in the systematic uncertainty. The statistical uncertainty on $F^{i}_{\rm norm}$ is negligible. Finally, $\langle T_{\rm pPb}\rangle$ is the centrality-dependent average nuclear thickness function, computed with the Glauber framework [45,47].

The systematic uncertainties entering the cross section and nuclear modification factor evaluation are summarised in Table 1.

When $R_{\rm pPb}$ is computed as a function of $p_{\rm T}$ or $y_{\rm cms}$, the systematic uncertainties on the signal extraction, tracking, trigger and matching efficiencies, MC input shapes and a fraction of the uncertainty on the pp reference are considered as bin-by-bin uncorrelated. On the contrary, the correlated contributions to the pp reference and the luminosity uncertainties, which are common to the p–Pb or Pb–p systems, are considered as correlated over $p_{\rm T}$ or $y_{\rm cms}$. In the $Q_{\rm pPb}$ evaluation, the uncertainties on signal extraction, on the MC input shapes and on $\langle T_{\rm pPb}\rangle$ depend on the centrality of the collision, while the other uncertainties are common to all classes and, therefore, considered as correlated over centrality. Even if most central events are not included in this analysis, a further 2% centrality-uncorrelated systematic uncertainty is assigned to the $Q_{\rm pPb}$ values, to account for residual pile-up which might still introduce a bias in the measurement. This systematic uncertainty is evaluated by comparing the expected pile-up fraction, computed from the pile-up probability associated to the observed interaction rate, and the amount of pile-up events removed by the event selection procedure. For the Υ(2S) and Υ(3S) studies, similar values of the systematic uncertainties are obtained, the main difference being the larger signal extraction uncertainties.

4. Results

The inclusive Υ(1S) production cross sections are evaluated in the rapidity regions $2.03 < y_{\rm cms} < 3.53$ and $-4.46 < y_{\rm cms} < -2.96$ and their values, computed according to Eq. (1), are:

Table 1
Systematic uncertainties, in percentage, on the three Υ cross sections and nuclear modification factors for both p–Pb and Pb–p collisions. Ranges in parentheses refer to the maximum variation as a function of centrality, y_{cms} or p_{T}. When no ranges are specified, the quoted values are valid for both the integrated and the differential measurements. Error type I means that the uncertainties are correlated over p_{T} or y_{cms}, while error type II refers to uncertainties correlated versus centrality. If no error type is specified, the uncertainties are considered as uncorrelated. The uncertainties on the pp reference and luminosity result from the combination of y_{cms}-uncorrelated and correlated contributions. For the systematic uncertainty on the luminosity determination, the two terms, defined according to [32], are separately quoted in the table, but combined when results are shown in the figures. Uncertainties on the B.R. are taken from [33].

Sources	Υ(1S)		Υ(2S)		Υ(3S)	
	p–Pb	Pb–p	p–Pb	Pb–p	p–Pb	Pb–p
Signal extraction	6.4 (5.1–15.9)	5.7 (5.5–8.5)	8.8	8.4	17.4	12.6
Trigger efficiency (II)	1.2 (1.1–1.3)	1.0 (1.0–1.1)	1.2	1.0	1.2	1.0
Tracking efficiency (II)	1.0	2.0	1.0	2.0	1.0	2.0
Matching efficiency (II)	1.0	1.0	1.0	1.0	1.0	1.0
MC inputs	1.0 (0.5–4.0)	1.0 (0.4–4.0)	1.3	1.6	1.4	1.8
pp reference (II)	0.2 (0.1–0.4)	0.2 (0.1–0.4)	0.2	0.3	0.2	0.2
pp reference (I,II)	2.8		2.8		2.8	
$\mathscr{L}_{\mathrm{int}}^{\mathrm{pPb}}$ (II)	2.1	2.2	2.1	2.2	2.1	2.2
$\mathscr{L}_{\mathrm{int}}^{\mathrm{pPb}}$ (I,II)	0.5	0.7	0.5	0.7	0.5	0.7
Pile-up	2.0	2.0	–		–	
$\langle T_{\mathrm{pPb}}\rangle$	2.1–5.8		–		–	
B.R. (I)	2.0		8.8		9.6	

$$\sigma_{\mathrm{pPb}}^{\Upsilon(1S)}(2.03 < y_{\mathrm{cms}} < 3.53)$$
$$= 14.5 \pm 1.0\ (\mathrm{stat.}) \pm 1.0\ (\mathrm{uncor.\,syst.}) \pm 0.3\ (\mathrm{cor.\,syst.})\ \mu\mathrm{b},$$
$$\sigma_{\mathrm{pPb}}^{\Upsilon(1S)}(-4.46 < y_{\mathrm{cms}} < -2.96)$$
$$= 10.5 \pm 0.6\ (\mathrm{stat.}) \pm 0.7\ (\mathrm{uncor.\,syst.}) \pm 0.2\ (\mathrm{cor.\,syst.})\ \mu\mathrm{b}.$$

The corresponding values for the Υ(2S) production cross sections are:

$$\sigma_{\mathrm{pPb}}^{\Upsilon(2S)}(2.03 < y_{\mathrm{cms}} < 3.53)$$
$$= 3.9 \pm 0.8\ (\mathrm{stat.}) \pm 0.4\ (\mathrm{uncor.\,syst.}) \pm 0.3\ (\mathrm{cor.\,syst.})\ \mu\mathrm{b},$$
$$\sigma_{\mathrm{pPb}}^{\Upsilon(2S)}(-4.46 < y_{\mathrm{cms}} < -2.96)$$
$$= 2.8 \pm 0.5\ (\mathrm{stat.}) \pm 0.3\ (\mathrm{uncor.\,syst.}) \pm 0.3\ (\mathrm{cor.\,syst.})\ \mu\mathrm{b},$$

and for the Υ(3S) are:

$$\sigma_{\mathrm{pPb}}^{\Upsilon(3S)}(2.03 < y_{\mathrm{cms}} < 3.53)$$
$$= 0.87 \pm 0.66\ (\mathrm{stat.}) \pm 0.15\ (\mathrm{uncor.\,syst.})$$
$$\pm 0.08\ (\mathrm{cor.\,syst.})\ \mu\mathrm{b},$$
$$\sigma_{\mathrm{pPb}}^{\Upsilon(3S)}(-4.46 < y_{\mathrm{cms}} < -2.96)$$
$$= 1.24 \pm 0.39\ (\mathrm{stat.}) \pm 0.15\ (\mathrm{uncor.\,syst.})$$
$$\pm 0.12\ (\mathrm{cor.\,syst.})\ \mu\mathrm{b}.$$

The systematic uncertainties have two terms, one correlated and one uncorrelated as a function of rapidity.

The data collected in p–Pb collisions at $\sqrt{s_{\mathrm{NN}}} = 8.16$ TeV allow for the measurement of the Υ(1S) production cross sections differentially in y_{cms} bins or in p_{T} intervals, up to $p_{\mathrm{T}} < 15$ GeV/c. The resulting cross sections are shown in Fig. 2 as a function of rapidity, integrated over transverse momentum, and in Fig. 3, as a function of p_{T}, in the forward- and backward-rapidity regions. In these figures, as in all the following ones, the statistical uncertainties are shown as vertical error bars, while the systematic uncertainties are represented as boxes around the points. The horizontal error bars correspond to the y_{cms} or p_{T} bin widths. The cross sections evaluated at forward and backward rapidities are compared with the pp ones, obtained through the aforementioned interpolation procedure, scaled by the Pb atomic mass number. The comparison shows that in the forward-rapidity region the Υ(1S) cross sections are smaller than the pp ones, in particular at low p_{T}, suggesting the presence of CNM effects at play in p–Pb collisions. On the contrary, in the backward-rapidity range the pp and the p–Pb cross

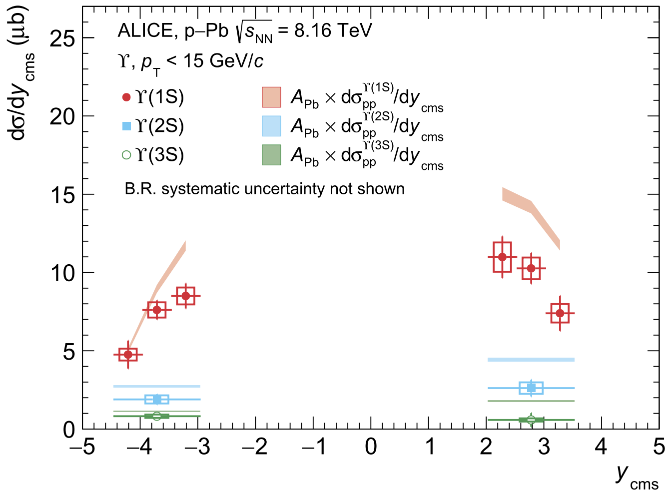

Fig. 2. Υ(1S), Υ(2S) and Υ(3S) differential cross sections as a function of y_{cms} in p–Pb collisions at $\sqrt{s_{\mathrm{NN}}} = 8.16$ TeV. The corresponding pp reference cross sections, obtained through the procedure described in Sec. 3 and scaled by A_{Pb}, are shown as bands.

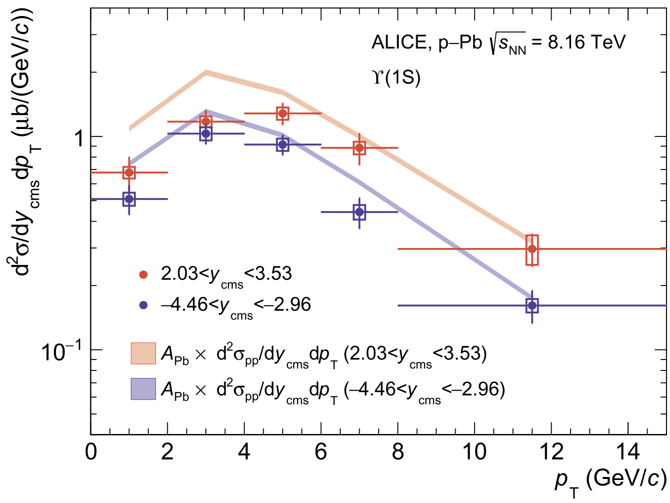

Fig. 3. Υ(1S) differential cross section as a function of p_{T}, at forward (closed symbols) and backward (open symbols) rapidity, at $\sqrt{s_{\mathrm{NN}}} = 8.16$ TeV. The pp reference cross section, obtained through the procedure described in Sec. 3 and scaled by A_{Pb}, is shown as a band.

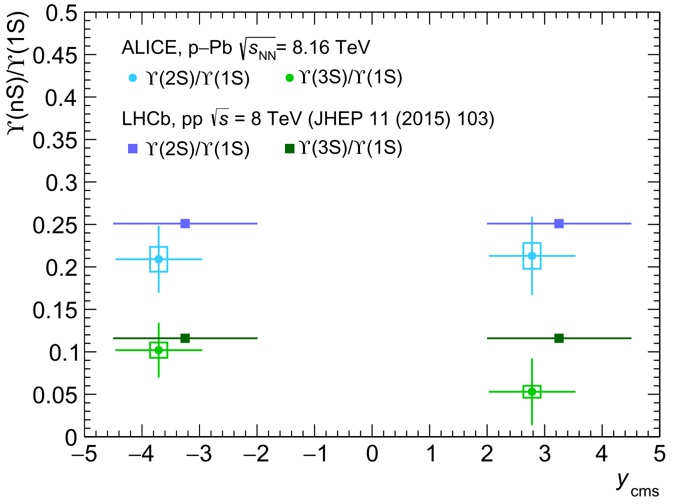

Fig. 4. Ratio of Υ(nS) over Υ(1S) yields in p–Pb collisions at $\sqrt{s_{\mathrm{NN}}} = 8.16$ TeV and in pp collisions at $\sqrt{s}$ = 8 TeV [36].

sections are closer and nuclear effects seem to have a less prominent role.

The limited available data sample allows for the evaluation of the Υ(2S) and Υ(3S) cross sections in the forward and backward-rapidity regions only integrating over the corresponding y_{cms} and p_{T} ranges, as shown in Fig. 2. A suppression with respect to the corresponding pp reference cross sections, scaled by A_{Pb}, is observed.

Given the relatively small mass difference between the Υ(1S) and Υ(2S) (or Υ(3S)) resonances, most of the systematic uncertainties, except those on the signal extraction and on the choice of the p_{T}- and y_{cms}-input shapes used in the MC, cancel in the ratio of the resonance yields, multiplied by their branching ratios, defined as

$$[\Upsilon(\mathrm{nS})/\Upsilon(1\mathrm{S})]_{\mathrm{pPb}} = \frac{N_{\Upsilon(\mathrm{nS})}/(A\times\varepsilon)_{\Upsilon(\mathrm{nS})}}{N_{\Upsilon(1\mathrm{S})}/(A\times\varepsilon)_{\Upsilon(1\mathrm{S})}}.$$

The values of the Υ(2S) over Υ(1S) ratio, obtained at forward and backward rapidity, are similar:

$$[\Upsilon(2\mathrm{S})/\Upsilon(1\mathrm{S})]_{\mathrm{pPb}}(2.03 < y_{\mathrm{cms}} < 3.53)$$
$$= 0.21 \pm 0.05\ (\mathrm{stat.}) \pm 0.02\ (\mathrm{syst.}),$$
$$[\Upsilon(2\mathrm{S})/\Upsilon(1\mathrm{S})]_{\mathrm{pPb}}(-4.46 < y_{\mathrm{cms}} < -2.96)$$
$$= 0.21 \pm 0.04\ (\mathrm{stat.}) \pm 0.01\ (\mathrm{syst.}).$$

As shown in Fig. 4, the ratio $[\Upsilon(2\mathrm{S})/\Upsilon(1\mathrm{S})]_{\mathrm{pPb}}$ at $\sqrt{s_{\mathrm{NN}}} = 8.16$ TeV is compatible, within uncertainties, with the results obtained by the LHCb Collaboration in pp collisions at $\sqrt{s}$ = 8 TeV [36], in a slightly wider kinematic range ($2 < y_{\mathrm{cms}} < 4.5$, $p_{\mathrm{T}} < 15$ GeV/c).

Similar conclusions can be obtained from the comparison of the Υ(3S) over Υ(1S) ratio, also shown in Fig. 4. The corresponding values at forward and backward rapidity are:

$$[\Upsilon(3\mathrm{S})/\Upsilon(1\mathrm{S})]_{\mathrm{pPb}}(2.03 < y_{\mathrm{cms}} < 3.53)$$
$$= 0.053 \pm 0.039\ (\mathrm{stat.}) \pm 0.007\ (\mathrm{syst.}),$$
$$[\Upsilon(3\mathrm{S})/\Upsilon(1\mathrm{S})]_{\mathrm{pPb}}(-4.46 < y_{\mathrm{cms}} < -2.96)$$
$$= 0.102 \pm 0.032\ (\mathrm{stat.}) \pm 0.009\ (\mathrm{syst.}).$$

The size of nuclear effects in p–Pb collisions can be better quantified through the nuclear modification factor defined in Eq. (2). The numerical values for the Υ(1S) R_{pPb} in the forward- and in the backward-rapidity regions, integrating over p_{T}, are:

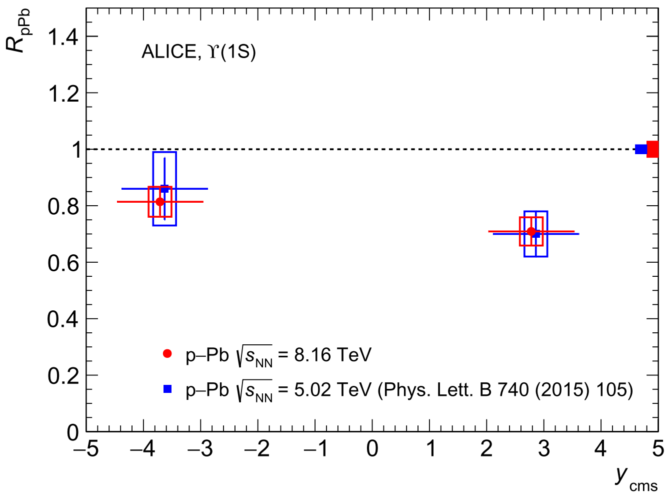

Fig. 5. Υ(1S) R_{pPb} values at $\sqrt{s_{\mathrm{NN}}} = 8.16$ TeV compared to those obtained at $\sqrt{s_{\mathrm{NN}}} = 5.02$ TeV in the same y_{cms} interval [18]. All systematic uncertainties are considered as uncorrelated between the results at $\sqrt{s_{\mathrm{NN}}} = 8.16$ TeV and $\sqrt{s_{\mathrm{NN}}} = 5.02$ TeV. The R_{pPb} values at the two energies are slightly displaced horizontally to improve visibility.

$$R^{\Upsilon(1\mathrm{S})}_{\mathrm{pPb}}(2.03 < y_{\mathrm{cms}} < 3.53)$$
$$= 0.71 \pm 0.05\ (\mathrm{stat.}) \pm 0.05\ (\mathrm{uncor.\,syst.}) \pm 0.02\ (\mathrm{cor.\,syst.}),$$
$$R^{\Upsilon(1\mathrm{S})}_{\mathrm{pPb}}(-4.46 < y_{\mathrm{cms}} < -2.96)$$
$$= 0.81 \pm 0.05\ (\mathrm{stat.}) \pm 0.05\ (\mathrm{uncor.\,syst.}) \pm 0.02\ (\mathrm{cor.\,syst.}),$$

where (uncor. syst.) and (cor. syst.) refer to uncorrelated and correlated systematic uncertainties as a function of rapidity.

The measured R_{pPb} values, shown in Fig. 5, indicate a suppression of the Υ(1S) production in p–Pb collisions, with respect to the one in pp collisions, both at forward and backward rapidity, with a slightly stronger suppression at forward y_{cms}. The R_{pPb} is found to be 4.0σ and 2.4σ below unity in p–Pb and Pb–p collisions, respectively. The results are compatible with the corresponding R_{pPb} values measured in p–Pb collisions at $\sqrt{s_{\mathrm{NN}}} = 5.02$ TeV [18], also shown in Fig. 5. From the comparison between the results obtained at the two energies, an improvement in the precision of the Υ(1S) R_{pPb} measurements at $\sqrt{s_{\mathrm{NN}}} = 8.16$ TeV can be noticed, given the reduced size of the statistical and systematic uncertainties. The improvement of the latter contribution is mainly related to the reduction in the uncertainties associated to the tracking efficiencies and to refinements in the determination of the pp reference [18].

The rapidity dependence of the Υ(1S) R_{pPb}, explored in narrower y_{cms} intervals, is shown in Fig. 6, confirming the suppression already observed in the y_{cms}-integrated case. The results are also compared with the Υ(1S) LHCb measurements [23] at the same centre-of-mass energy and in slightly wider kinematic ranges ($-4.5 < y_{\mathrm{cms}} < -2.5$ and $2 < y_{\mathrm{cms}} < 4$, $p_{\mathrm{T}} < 25$ GeV/c). Fair agreement between the two sets of results can be seen.

The p_{T} dependence of the Υ(1S) R_{pPb} is shown in Fig. 7. A slight decrease of the Υ(1S) nuclear modification factor, with decreasing p_{T}, is observed. The behaviour is similar both at backward and forward rapidities.

The y_{cms} and p_{T} dependence of the Υ(1S) R_{pPb} are compared, in Fig. 6 and Fig. 7, to several models (referred in the following as nuclear shadowing models), based on EPS09 [8], nCTEQ15 [10] or EPPS16 [9] sets of nuclear parton distribution functions. The EPS09 next-to-leading order (NLO) parametrisation is combined with a NLO Colour Evaporation Model (CEM) [48], which describes the Υ production. The corresponding uncertainty bands, shown in Fig. 6 and Fig. 7, are dominated by the uncertainties of the EPS09 parametrisation. The nCTEQ15 and the EPPS16 NLO nPDFs

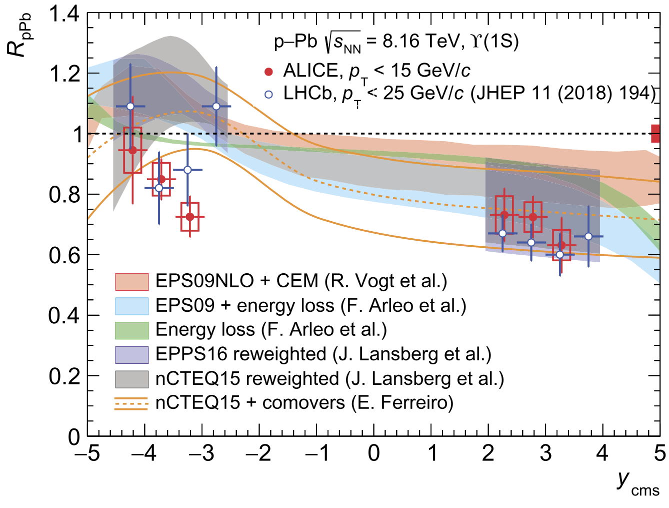

Fig. 6. ϒ(1S) R_{pPb} values at $\sqrt{s_{NN}} = 8.16$ TeV compared with the corresponding LHCb results [23], as a function of y_{cms}. The R_{pPb} values are also compared to model calculations based on several implementations of nuclear shadowing (EPS09 NLO [8,14,48], EPPS16 and nCTEQ15 [9–11,49–51]) and on parton coherent energy loss predictions, with or without the inclusion of the EPS09 shadowing contribution [13,14]. A theoretical model including a shadowing contribution based on nCTEQ15 nPDFs on top of a suppression induced by comover interactions [15,52] is also shown. For the LHCb results, the vertical error bars represent the quadratic sum of the statistical and systematic uncertainties.

sets are implemented following the Bayesian reweighting procedure described in [11,49–51]. The uncertainty bands, in this case, represent the convolution of the uncertainties on the nPDFs sets and those on the factorisation scales. It can be observed that the shadowing calculations describe fairly well the p_T and y_{cms} dependence of the ϒ(1S) nuclear modification factor in $2.03 < y_{cms} < 3.05$, while they overestimate the results obtained in $-4.46 < y_{cms} < -2.96$. Furthermore, while the p_T dependence of the ALICE measurements indicate slightly stronger cold nuclear matter effects at low p_T, the shadowing calculations suggest a flatter behaviour. Finally, the y_{cms} dependence of the R_{pPb} is also compared with a model which includes the effects of parton coherent energy loss with or without the contribution of the EPS09 nuclear shadowing [13,14]. The model predicts a mild dependence of the energy loss mechanism on rapidity. When the nuclear shadowing contribution is included, the model describes the forward-rapidity results, while it slightly overestimates the backward-rapidity R_{pPb}. The ϒ(1S) R_{pPb} is also compared with a theoretical model which includes a shadowing contribution, based on the nCTEQ15 set of nPDFs, on top of a suppression of the ϒ(1S) production due to interactions with comoving particles [15,52]. The uncertainties associated to this theoretical calculation include a small contribution from the uncertainty on the comovers cross section and are dominated by the uncertainties on the shadowing. Also in this case the calculation slightly overestimates the ALICE measurements at backward y_{cms}, while at forward y_{cms} the data agree with the model. It can be noted that the interpretation of the ϒ(1S) behaviour in p–Pb collisions would also benefit from a precise knowledge, so far still affected by large uncertainties, of the feed-down contribution of the excited states into the ϒ(1S).

The ϒ(1S) nuclear modification factor is evaluated as a function of the collision centrality. The Q_{pPb} results, shown in Fig. 8, are presented as a function of the average number of collisions, $\langle N_{coll} \rangle$ and it can be observed that both at forward and backward rapidity the ϒ(1S) centrality dependence is rather flat.

Finally, the nuclear modification factor is also evaluated for the ϒ(2S) and ϒ(3S) resonances, in the forward and backward-y_{cms} intervals, as shown in Fig. 9. The corresponding ϒ(2S) R_{pPb} values are:

$$R_{pPb}^{\Upsilon(2S)}(2.03 < y_{cms} < 3.53)$$
$$= 0.59 \pm 0.12\,(\text{stat.}) \pm 0.05\,(\text{uncor. syst.}) \pm 0.02\,(\text{cor. syst.})$$
$$R_{pPb}^{\Upsilon(2S)}(-4.46 < y_{cms} < -2.96)$$
$$= 0.69 \pm 0.12\,(\text{stat.}) \pm 0.05\,(\text{uncor. syst.}) \pm 0.02\,(\text{cor. syst.})$$

the ϒ(2S) suppression being compatible with unity within 3.1σ at forward y_{cms} and 2.3σ at backward y_{cms}. The ϒ(3S) R_{pPb} values are:

$$R_{pPb}^{\Upsilon(3S)}(2.03 < y_{cms} < 3.53)$$
$$= 0.32 \pm 0.24\,(\text{stat.}) \pm 0.06\,(\text{uncor. syst.}) \pm 0.01\,(\text{cor. syst.})$$
$$R_{pPb}^{\Upsilon(3S)}(-4.46 < y_{cms} < -2.96)$$
$$= 0.71 \pm 0.23\,(\text{stat.}) \pm 0.09\,(\text{uncor. syst.}) \pm 0.02\,(\text{cor. syst.})$$

The ϒ(3S) suppression is compatible with unity within 2.7σ at forward y_{cms} and 1.2σ at backward y_{cms}. The difference in the R_{pPb} of the ϒ(2S) and ϒ(1S) amounts to 0.5σ in both rapidity intervals, suggesting, in p–Pb collisions, a similar modification of the production yields of the two ϒ states, with respect to pp collisions. Unfortunately, the large uncertainties on the ϒ(3S) prevent robust conclusions on the behaviour of the most loosely bound bottomonium state. The model which includes both the nuclear shadowing contribution (nCTEQ15) and interactions with comoving particles [15,52] suggests a small difference between the nuclear modification factors of the three ϒ states. This difference is slightly more important in the backward-rapidity range, while it becomes negligible at forward y_{cms}. By evaluating the ratio of the ϒ(nS) to ϒ(1S) nuclear modification factors, the shadowing contribution and most of the theory uncertainties, as well as some of the uncertainties on the data, cancel out. The shape of the theoretical calculation is, hence, mainly driven by the interactions with the comoving particles, which affect mostly the excited ϒ states in the backward rapidity region. As shown in the lower panel of Fig. 9, the ALICE measurements and the model are in fair agreement, even if the uncertainties on the data do not yet allow a firm conclusion on the role of comovers to be drawn.

5. Conclusions

The ALICE measurements of the rapidity, transverse momentum and centrality dependence of the inclusive ϒ(1S) nuclear modification factor in p–Pb collisions at $\sqrt{s_{NN}} = 8.16$ TeV have been presented. The results show a suppression of the ϒ(1S) yields, with respect to the ones measured in pp collisions at the same centre-of-mass energy. The R_{pPb} values are similar at forward and backward rapidity with a slightly stronger suppression at low p_T, while in both rapidity intervals there is no evidence for a centrality dependence of the ϒ(1S) Q_{pPb}. The results obtained at $\sqrt{s_{NN}} = 8.16$ TeV are similar within uncertainties to those measured by ALICE in p–Pb collisions at the lower energy of $\sqrt{s_{NN}} = 5.02$ TeV and show a good agreement with the LHCb measurements at the same centre-of-mass energy. Models based on nuclear shadowing, coherent parton energy loss or interactions with comoving particles fairly describe the data at forward rapidity, while they tend to overestimate the R_{pPb} at backward y_{cms}. The ϒ(2S) R_{pPb} has also been measured, showing a strong suppression, similar to the one measured for the ϒ(1S) in the two investigated rapidity intervals. Finally, a first measurement of the ϒ(3S) has also been performed, even if the large uncertainties prevent a detailed comparison of its behaviour in p–Pb collisions with respect to the other bottomonium states. These new bottomonium measurements represent an

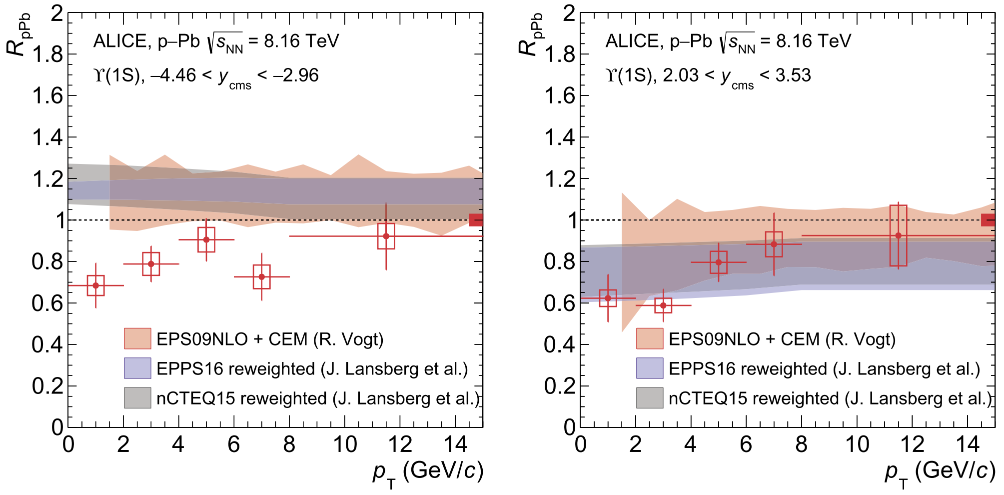

Fig. 7. Υ(1S) R_{pPb} as a function of p_T for Pb–p (left panel) and p–Pb collisions (right panel). The R_{pPb} values are compared with theoretical calculations based on EPS09 NLO [14,48], nCTEQ15 and EPPS16 [9–11,49–51] shadowing implementations. Details on the theory uncertainty bands are discussed in the text.

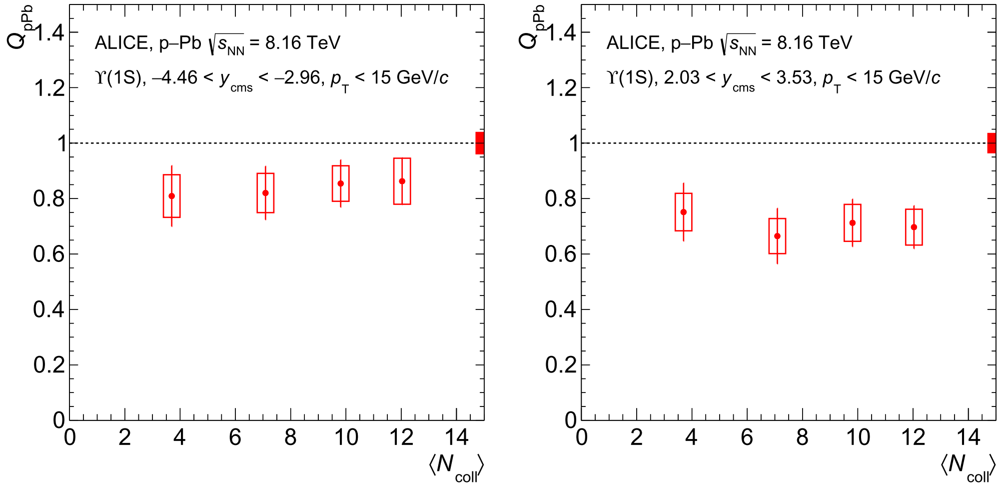

Fig. 8. Υ(1S) Q_{pPb} as a function of $\langle N_{coll} \rangle$, for Pb–p (left panel) and p–Pb collisions (right panel).

important baseline for the understanding of the role of CNM effects in p–Pb collisions and open up the way for future precision analyses with the upcoming LHC Run 3 and Run 4 data taking periods.

Declaration of competing interest

The authors declare that they have no known competing financial interests or personal relationships that could have appeared to influence the work reported in this paper.

Acknowledgements

The ALICE Collaboration would like to thank all its engineers and technicians for their invaluable contributions to the construction of the experiment and the CERN accelerator teams for the outstanding performance of the LHC complex. The ALICE Collaboration gratefully acknowledges the resources and support provided by all Grid centres and the Worldwide LHC Computing Grid (WLCG) collaboration. The ALICE Collaboration acknowledges the following funding agencies for their support in building and running the ALICE detector: A. I. Alikhanyan National Science Laboratory (Yerevan Physics Institute) Foundation (ANSL), State Committee of Science and World Federation of Scientists (WFS), Armenia; Austrian Academy of Sciences, Austrian Science Fund (FWF): [M 2467-N36] and Nationalstiftung für Forschung, Technologie und Entwicklung, Austria; Ministry of Communications and High Technologies, National Nuclear Research Center, Azerbaijan; Conselho Nacional de Desenvolvimento Científico e Tecnológico (CNPq), Financiadora de Estudos e Projetos (Finep), Fundação de Amparo à Pesquisa do Estado de São Paulo (FAPESP) and Universidade Federal do Rio Grande do Sul (UFRGS), Brazil; Ministry of Education of China (MOEC), Ministry of Science & Technology of China (MSTC) and National Natural Science Foundation of China (NSFC), China; Ministry of Science and Education and Croatian Science Foundation, Croatia; Centro de Aplicaciones Tecnológicas y Desarrollo Nuclear (CEADEN), Cubaenergía, Cuba; Ministry of Education, Youth and Sports of the Czech Republic, Czech Republic; The Danish Council for Independent Research | Natural Sciences, the Villum Fonden and Danish National Research Foundation (DNRF), Denmark; Helsinki Institute of Physics (HIP), Finland; Commissariat à l'Énergie Atomique (CEA), Institut National de Physique Nucléaire et de Physique des Particules (IN2P3) and Centre National de la Recherche Scientifique (CNRS) and Région des Pays de la Loire, France; Bundesministerium für Bildung und Forschung (BMBF) and GSI Helmholtzzentrum für Schwerionenforschung GmbH, Germany; General Secretariat for Research and Technology, Ministry of

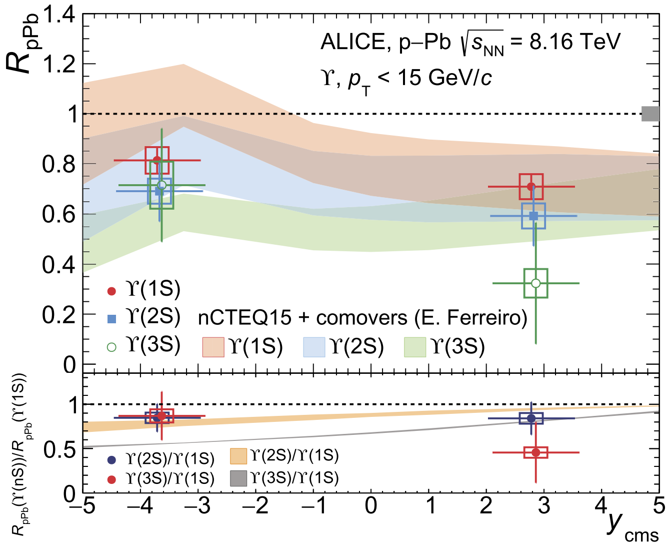

Fig. 9. Υ(1S), Υ(2S) and Υ(3S) $R_{\rm pPb}$ at $\sqrt{s_{\rm NN}} = 8.16$ TeV as a function of $y_{\rm cms}$. The $R_{\rm pPb}$ values of the three resonances are slightly displaced horizontally to improve visibility. Theoretical calculations including nCTEQ15 shadowing contribution and interactions between the Υ states and comoving particles [15,52] are also shown for all the resonances. The grey box around unity represents the global uncertainty common to the three Υ states. In the lower panel, the ratio of the Υ(2S) to Υ(1S) and Υ(3S) to Υ(1S) $R_{\rm pPb}$ is shown, together with a calculation based on the aforementioned theory model [15,52].

Education, Research and Religions, Greece; National Research Development and Innovation Office, Hungary; Department of Atomic Energy, Government of India (DAE), Department of Science and Technology, Government of India (DST), University Grants Commission, Government of India (UGC) and Council of Scientific and Industrial Research (CSIR), India; Indonesian Institute of Science, Indonesia; Centro Fermi - Museo Storico della Fisica e Centro Studi e Ricerche Enrico Fermi and Istituto Nazionale di Fisica Nucleare (INFN), Italy; Institute for Innovative Science and Technology, Nagasaki Institute of Applied Science (IIST), Japanese Ministry of Education, Culture, Sports, Science and Technology (MEXT) and Japan Society for the Promotion of Science (JSPS) KAKENHI, Japan; Consejo Nacional de Ciencia (CONACYT) y Tecnología, through Fondo de Cooperación Internacional en Ciencia y Tecnología (FONCICYT) and Dirección General de Asuntos del Personal Academico (DGAPA), Mexico; Nederlandse Organisatie voor Wetenschappelijk Onderzoek (NWO), Netherlands; The Research Council of Norway, Norway; Commission on Science and Technology for Sustainable Development in the South (COMSATS), Pakistan; Pontificia Universidad Católica del Perú, Peru; Ministry of Science and Higher Education and National Science Centre, Poland; Korea Institute of Science and Technology Information and National Research Foundation of Korea (NRF), Republic of Korea; Ministry of Education and Scientific Research, Institute of Atomic Physics and Ministry of Research and Innovation and Institute of Atomic Physics, Romania; Joint Institute for Nuclear Research (JINR), Ministry of Education and Science of the Russian Federation, National Research Centre Kurchatov Institute, Russian Science Foundation and Russian Foundation for Basic Research, Russia; Ministry of Education, Science, Research and Sport of the Slovak Republic, Slovakia; National Research Foundation of South Africa, South Africa; Swedish Research Council (VR) and Knut & Alice Wallenberg Foundation (KAW), Sweden; European Organization for Nuclear Research, Switzerland; Suranaree University of Technology (SUT), National Science and Technology Development Agency (NSDTA) and Office of the Higher Education Commission under NRU project of Thailand, Thailand; Turkish Atomic Energy Agency (TAEK), Turkey; National Academy of Sciences of Ukraine, Ukraine; Science and Technology Facilities Council (STFC), United Kingdom; National Science Foundation of the United States of America (NSF) and United States Department of Energy, Office of Nuclear Physics (DOE NP), United States of America.

References

[1] T. Matsui, H. Satz, J/ψ suppression by quark-gluon plasma formation, Phys. Lett. B 178 (1986) 416–422.
[2] ALICE Collaboration, B.B. Abelev, et al., Suppression of $\Upsilon(1S)$ at forward rapidity in Pb-Pb collisions at $\sqrt{s_{\rm NN}} = 2.76$ TeV, Phys. Lett. B 738 (2014) 361–372, arXiv:1405.4493 [nucl-ex].
[3] ALICE Collaboration, S. Acharya, et al., Υ suppression at forward rapidity in Pb-Pb collisions at $\sqrt{s_{\rm NN}} = 5.02$ TeV, Phys. Lett. B 790 (2019) 89–101, arXiv:1805.04387 [nucl-ex].
[4] CMS Collaboration, S. Chatrchyan, et al., Indications of suppression of excited Υ states in PbPb collisions at $\sqrt{S_{NN}} = 2.76$ TeV, Phys. Rev. Lett. 107 (2011) 052302, arXiv:1105.4894 [nucl-ex].
[5] CMS Collaboration, S. Chatrchyan, et al., Observation of sequential Υ suppression in PbPb collisions, Phys. Rev. Lett. 109 (2012) 222301, arXiv:1208.2826 [nucl-ex].
[6] CMS Collaboration, A.M. Sirunyan, et al., Measurement of nuclear modification factors of Υ(1S), Υ(2S), and Υ(3S) mesons in PbPb collisions at $\sqrt{s_{\rm NN}} = 5.02$ TeV, Phys. Lett. B 790 (2019) 270–293, arXiv:1805.09215 [hep-ex].
[7] H. Satz, Quarkonium binding and dissociation: the spectral analysis of the QGP, Nucl. Phys. A 783 (2007) 249–260, arXiv:hep-ph/0609197 [hep-ph].
[8] K.J. Eskola, H. Paukkunen, C.A. Salgado, EPS09: a new generation of NLO and LO nuclear parton distribution functions, J. High Energy Phys. 04 (2009) 065, arXiv:0902.4154 [hep-ph].
[9] K.J. Eskola, P. Paakkinen, H. Paukkunen, C.A. Salgado, EPPS16: nuclear parton distributions with LHC data, Eur. Phys. J. C 77 (3) (2017) 163, arXiv:1612.05741 [hep-ph].
[10] K. Kovarik, et al., nCTEQ15 - global analysis of nuclear parton distributions with uncertainties in the CTEQ framework, Phys. Rev. D 93 (8) (2016) 085037, arXiv:1509.00792 [hep-ph].
[11] A. Kusina, J.P. Lansberg, I. Schienbein, H.-S. Shao, Gluon shadowing in heavy-flavor production at the LHC, Phys. Rev. Lett. 121 (5) (2018) 052004, arXiv:1712.07024 [hep-ph].
[12] H. Fujii, K. Watanabe, Heavy quark pair production in high energy pA collisions: quarkonium, Nucl. Phys. A 915 (2013) 1–23, arXiv:1304.2221 [hep-ph].
[13] F. Arleo, S. Peigné, Heavy-quarkonium suppression in p-A collisions from parton energy loss in cold QCD matter, J. High Energy Phys. 03 (2013) 122, arXiv:1212.0434 [hep-ph].
[14] J.L. Albacete, et al., Predictions for cold nuclear matter effects in p+Pb collisions at $\sqrt{s_{NN}} = 8.16$ TeV, Nucl. Phys. A 972 (2018) 18–85, arXiv:1707.09973 [hep-ph].
[15] E.G. Ferreiro, J.P. Lansberg, Is bottomonium suppression in proton-nucleus and nucleus-nucleus collisions at LHC energies due to the same effects?, J. High Energy Phys. 10 (2018) 094, arXiv:1804.04474 [hep-ph], Erratum: J. High Energy Phys. 03 (2019) 063.
[16] E.G. Ferreiro, Charmonium dissociation and recombination at LHC: revisiting comovers, Phys. Lett. B 731 (2014) 57–63, arXiv:1210.3209 [hep-ph].
[17] X. Du, R. Rapp, In-medium charmonium production in proton-nucleus collisions, J. High Energy Phys. 03 (2019) 015, arXiv:1808.10014 [nucl-th].
[18] ALICE Collaboration, B.B. Abelev, et al., Production of inclusive Υ(1S) and Υ(2S) in p-Pb collisions at $\sqrt{s_{\rm NN}} = \mathbf{5.02}$ TeV, Phys. Lett. B 740 (2015) 105–117, arXiv:1410.2234 [nucl-ex].
[19] ALICE Collaboration, B.B. Abelev, et al., Measurement of quarkonium production at forward rapidity in pp collisions at $\sqrt{s} = 7$ TeV, Eur. Phys. J. C 74 (8) (2014) 2974, arXiv:1403.3648 [nucl-ex].
[20] LHCb Collaboration, R. Aaij, et al., Study of Υ production and cold nuclear matter effects in pPb collisions at $\sqrt{s_{NN}} = 5$ TeV, J. High Energy Phys. 07 (2014) 094, arXiv:1405.5152 [nucl-ex].
[21] ATLAS Collaboration, M. Aaboud, et al., Measurement of quarkonium production in proton–lead and proton–proton collisions at 5.02 TeV with the ATLAS detector, Eur. Phys. J. C 78 (3) (2018) 171, arXiv:1709.03089 [nucl-ex].
[22] CMS Collaboration, S. Chatrchyan, et al., Event activity dependence of Y(nS) production in $\sqrt{s_{NN}} = 5.02$ TeV pPb and $\sqrt{s} = 2.76$ TeV pp collisions, J. High Energy Phys. 04 (2014) 103, arXiv:1312.6300 [nucl-ex].
[23] LHCb Collaboration, R. Aaij, et al., Study of Υ production in pPb collisions at $\sqrt{s_{NN}} = 8.16$ TeV, J. High Energy Phys. 11 (2018) 194, arXiv:1810.07655 [hep-ex].
[24] ALICE Collaboration, K. Aamodt, et al., The ALICE experiment at the CERN LHC, J. Instrum. 3 (2008) S08002.
[25] ALICE Collaboration, B.B. Abelev, et al., Performance of the ALICE experiment at the CERN LHC, Int. J. Mod. Phys. A 29 (2014) 1430044, arXiv:1402.4476 [nucl-ex].
[26] ALICE Collaboration, Technical design report of the dimuon forward spectrometer, https://edms.cern.ch/document/470838/1.

[27] ALICE Collaboration, K. Aamodt, et al., Alignment of the ALICE inner tracking system with cosmic-ray tracks, J. Instrum. 5 (2010) P03003, arXiv:1001.0502 [physics.ins-det].

[28] ALICE Collaboration, E. Abbas, et al., Performance of the ALICE VZERO system, J. Instrum. 8 (2013) P10016, arXiv:1306.3130 [nucl-ex].

[29] M. Bondila, et al., ALICE T0 detector, IEEE Trans. Nucl. Sci. 52 (2005) 1705–1711.

[30] ALICE Collaboration, B. Abelev, et al., Measurement of the cross section for electromagnetic dissociation with neutron emission in Pb-Pb collisions at $\sqrt{s_{NN}} = 2.76$ TeV, Phys. Rev. Lett. 109 (2012) 252302, arXiv:1203.2436 [nucl-ex].

[31] ALICE Collaboration, S. Acharya, et al., Inclusive J/ψ production at forward and backward rapidity in p-Pb collisions at $\sqrt{s_{\rm NN}} = 8.16$ TeV, J. High Energy Phys. 07 (2018) 160, arXiv:1805.04381 [nucl-ex].

[32] ALICE Collaboration, S. Acharya, et al., ALICE luminosity determination for p-Pb and Pb-p collisions at $\sqrt{s_{\rm NN}} = 8.16$ TeV, ALICE-PUBLIC-2018-002, https://cds.cern.ch/record/2314660.

[33] Particle Data Group Collaboration, M. Tanabashi, et al., Review of particle physics, Phys. Rev. D 98 (3) (2018) 030001.

[34] ALICE Collaboration, J. Adam, et al., Quarkonium signal extraction in ALICE, ALICE-PUBLIC-2015-006, https://cds.cern.ch/record/2060096.

[35] R. Brun, et al., GEANT3 detector description and simulation tool, CERN Program Library, CERN-W5013, https://cds.cern.ch/record/1082634.

[36] LHCb Collaboration, R. Aaij, et al., Forward production of Υ mesons in pp collisions at $\sqrt{s} = 7$ and 8 TeV, J. High Energy Phys. 11 (2015) 103, arXiv:1509.02372 [hep-ex].

[37] CDF Collaboration, D. Acosta, et al., Υ production and polarization in $p\bar{p}$ collisions at $\sqrt{s} = 1.8$-TeV, Phys. Rev. Lett. 88 (2002) 161802.

[38] LHCb Collaboration, R. Aaij, et al., Measurement of Υ production in pp collisions at $\sqrt{s} = 7$ TeV, Eur. Phys. J. C 72 (2012) 2025, arXiv:1202.6579 [hep-ex].

[39] CMS Collaboration, V. Khachatryan, et al., Υ production cross-section in pp collisions at $sqrts = 7$ TeV, Phys. Rev. D 83 (2011) 112004, arXiv:1012.5545 [hep-ex].

[40] F. Bossu, Z.C. del Valle, A. de Falco, M. Gagliardi, S. Grigoryan, G. Martinez Garcia, Phenomenological interpolation of the inclusive J/ψ cross section to proton-proton collisions at 2.76 TeV and 5.5 TeV, arXiv:1103.2394 [nucl-ex].

[41] ALICE Collaboration, B.B. Abelev, et al., J/ψ production and nuclear effects in p-Pb collisions at $\sqrt{s_{NN}} = 5.02$ TeV, J. High Energy Phys. 02 (2014) 073, arXiv:1308.6726 [nucl-ex].

[42] LHCb Collaboration, R. Aaij, et al., Measurement of Υ production in pp collisions at $\sqrt{s} = 13$ TeV, J. High Energy Phys. 07 (2018) 134, arXiv:1804.09214 [hep-ex].

[43] ALICE Collaboration, J. Adam, et al., Reference pp cross-sections for Υ(1S) studies in pPb collisions at $\sqrt{s_{\rm NN}} = 5.02$ TeV and comparisons between ALICE and LHCb results, ALICE-PUBLIC-2014-002, https://cds.cern.ch/record/2314660.

[44] ALICE Collaboration, J. Adam, et al., Inclusive quarkonium production at forward rapidity in pp collisions at $\sqrt{s} = 8$ TeV, Eur. Phys. J. C 76 (4) (2016) 184, arXiv:1509.08258 [hep-ex].

[45] ALICE Collaboration, J. Adam, et al., Centrality dependence of particle production in p-Pb collisions at $\sqrt{s_{\rm NN}} = 5.02$ TeV, Phys. Rev. C 91 (6) (2015) 064905, arXiv:1412.6828 [nucl-ex].

[46] ALICE Collaboration, J. Adam, et al., Centrality dependence of inclusive J/ψ production in p-Pb collisions at $\sqrt{s_{\rm NN}} = 5.02$ TeV, J. High Energy Phys. 11 (2015) 127, arXiv:1506.08808 [nucl-ex].

[47] M.L. Miller, K. Reygers, S.J. Sanders, P. Steinberg, Glauber modeling in high energy nuclear collisions, Annu. Rev. Nucl. Part. Sci. 57 (2007) 205–243, arXiv:nucl-ex/0701025 [nucl-ex].

[48] R. Vogt, Shadowing effects on J/ψ and Υ production at energies available at the CERN large hadron collider, Phys. Rev. C 92 (3) (2015) 034909, arXiv:1507.04418 [hep-ph].

[49] J.P. Lansberg, H.S. Shao, Towards an automated tool to evaluate the impact of the nuclear modification of the gluon density on quarkonium, D and B meson production in proton–nucleus collisions, Eur. Phys. J. C 77 (1) (2017) 1, arXiv:1610.05382 [hep-ph].

[50] H.S. Shao, HELAC-Onia 2.0: an upgraded matrix-element and event generator for heavy qurakonium physics, Comput. Phys. Commun. 198 (2016) 238–259, arXiv:1507.03435 [hep-ph].

[51] H.S. Shao, HELAC-Onia: an automatic matrix element generator for heavy quarkonium physics, Comput. Phys. Commun. 184 (2013) 2562–2570, arXiv:1212.5293 [hep-ph].

[52] E.G. Ferreiro, Global description of bottomonium suppression in proton-nucleus and nucleus-nucleus collisions at LHC energies, PoS DIS2018 (2018) 130, arXiv:1810.12874 [hep-ph].

ALICE Collaboration

S. Acharya[141], D. Adamová[94], A. Adler[74], J. Adolfsson[80], M.M. Aggarwal[99], G. Aglieri Rinella[33], M. Agnello[30], N. Agrawal[10,53], Z. Ahammed[141], S. Ahmad[16], S.U. Ahn[76], A. Akindinov[91], M. Al-Turany[106], S.N. Alam[141], D.S.D. Albuquerque[122], D. Aleksandrov[87], B. Alessandro[58], H.M. Alfanda[6], R. Alfaro Molina[71], B. Ali[16], Y. Ali[14], A. Alici[10,26,53], A. Alkin[2], J. Alme[21], T. Alt[68], L. Altenkamper[21], I. Altsybeev[112], M.N. Anaam[6], C. Andrei[47], D. Andreou[33], H.A. Andrews[110], A. Andronic[144], M. Angeletti[33], V. Anguelov[103], C. Anson[15], T. Antičić[107], F. Antinori[56], P. Antonioli[53], R. Anwar[125], N. Apadula[79], L. Aphecetche[114], H. Appelshäuser[68], S. Arcelli[26], R. Arnaldi[58], M. Arratia[79], I.C. Arsene[20], M. Arslandok[103], A. Augustinus[33], R. Averbeck[106], S. Aziz[61], M.D. Azmi[16], A. Badalà[55], Y.W. Baek[40], S. Bagnasco[58], X. Bai[106], R. Bailhache[68], R. Bala[100], A. Baldisseri[137], M. Ball[42], S. Balouza[104], R. Barbera[27], L. Barioglio[25], G.G. Barnaföldi[145], L.S. Barnby[93], V. Barret[134], P. Bartalini[6], K. Barth[33], E. Bartsch[68], F. Baruffaldi[28], N. Bastid[134], S. Basu[143], G. Batigne[114], B. Batyunya[75], D. Bauri[48], J.L. Bazo Alba[111], I.G. Bearden[88], C. Bedda[63], N.K. Behera[60], I. Belikov[136], A.D.C. Bell Hechavarria[144], F. Bellini[33], R. Bellwied[125], V. Belyaev[92], G. Bencedi[145], S. Beole[25], A. Bercuci[47], Y. Berdnikov[97], D. Berenyi[145], R.A. Bertens[130], D. Berzano[58], M.G. Besoiu[67], L. Betev[33], A. Bhasin[100], I.R. Bhat[100], M.A. Bhat[3], H. Bhatt[48], B. Bhattacharjee[41], A. Bianchi[25], L. Bianchi[25], N. Bianchi[51], J. Bielčík[36], J. Bielčíková[94], A. Bilandzic[104,117], G. Biro[145], R. Biswas[3], S. Biswas[3], J.T. Blair[119], D. Blau[87], C. Blume[68], G. Boca[139], F. Bock[33,95], A. Bogdanov[92], S. Boi[23], L. Boldizsár[145], A. Bolozdynya[92], M. Bombara[37], G. Bonomi[140], H. Borel[137], A. Borissov[92,144], H. Bossi[146], E. Botta[25], L. Bratrud[68], P. Braun-Munzinger[106], M. Bregant[121], M. Broz[36], E.J. Brucken[43], E. Bruna[58], G.E. Bruno[105], M.D. Buckland[127], D. Budnikov[108], H. Buesching[68], S. Bufalino[30], O. Bugnon[114], P. Buhler[113], P. Buncic[33], Z. Buthelezi[72,131], J.B. Butt[14], J.T. Buxton[96], S.A. Bysiak[118], D. Caffarri[89], A. Caliva[106], E. Calvo Villar[111], R.S. Camacho[44], P. Camerini[24], A.A. Capon[113], F. Carnesecchi[10,26], R. Caron[137], J. Castillo Castellanos[137], A.J. Castro[130], E.A.R. Casula[54], F. Catalano[30], C. Ceballos Sanchez[52], P. Chakraborty[48], S. Chandra[141], W. Chang[6], S. Chapeland[33], M. Chartier[127], S. Chattopadhyay[141], S. Chattopadhyay[109], A. Chauvin[23], C. Cheshkov[135], B. Cheynis[135], V. Chibante Barroso[33], D.D. Chinellato[122], S. Cho[60], P. Chochula[33], T. Chowdhury[134], P. Christakoglou[89], C.H. Christensen[88], P. Christiansen[80], T. Chujo[133], C. Cicalo[54], L. Cifarelli[10,26], F. Cindolo[53], J. Cleymans[124], F. Colamaria[52], D. Colella[52], A. Collu[79], M. Colocci[26], M. Concas[58,ii], G. Conesa Balbastre[78], Z. Conesa del Valle[61], G. Contin[24,127], J.G. Contreras[36], T.M. Cormier[95], Y. Corrales Morales[25], P. Cortese[31], M.R. Cosentino[123], F. Costa[33], S. Costanza[139], P. Crochet[134], E. Cuautle[69], P. Cui[6], L. Cunqueiro[95], D. Dabrowski[142], T. Dahms[104,117], A. Dainese[56], F.P.A. Damas[114,137], M.C. Danisch[103], A. Danu[67], D. Das[109], I. Das[109], P. Das[85], P. Das[3], S. Das[3], A. Dash[85], S. Dash[48], S. De[85], A. De Caro[29], G. de Cataldo[52], J. de Cuveland[38], A. De Falco[23], D. De Gruttola[10], N. De Marco[58], S. De Pasquale[29], S. Deb[49], B. Debjani[3], H.F. Degenhardt[121], K.R. Deja[142], A. Deloff[84], S. Delsanto[25,131], D. Devetak[106], P. Dhankher[48], D. Di Bari[32], A. Di Mauro[33], R.A. Diaz[8], T. Dietel[124], P. Dillenseger[68], Y. Ding[6], R. Divià[33], D.U. Dixit[19], Ø. Djuvsland[21], U. Dmitrieva[62], A. Dobrin[33,67], B. Dönigus[68], O. Dordic[20], A.K. Dubey[141], A. Dubla[106], S. Dudi[99], M. Dukhishyam[85], P. Dupieux[134], R.J. Ehlers[146], V.N. Eikeland[21], D. Elia[52], H. Engel[74], E. Epple[146], B. Erazmus[114], F. Erhardt[98], A. Erokhin[112], M.R. Ersdal[21], B. Espagnon[61], G. Eulisse[33], D. Evans[110], S. Evdokimov[90], L. Fabbietti[104,117], M. Faggin[28], J. Faivre[78], F. Fan[6], A. Fantoni[51], M. Fasel[95], P. Fecchio[30], A. Feliciello[58], G. Feofilov[112], A. Fernández Téllez[44], A. Ferrero[137], A. Ferretti[25], A. Festanti[33], V.J.G. Feuillard[103], J. Figiel[118], S. Filchagin[108], D. Finogeev[62], F.M. Fionda[21], G. Fiorenza[52], F. Flor[125], S. Foertsch[72], P. Foka[106], S. Fokin[87], E. Fragiacomo[59], U. Frankenfeld[106], U. Fuchs[33], C. Furget[78], A. Furs[62], M. Fusco Girard[29], J.J. Gaardhøje[88], M. Gagliardi[25], A.M. Gago[111], A. Gal[136], C.D. Galvan[120], P. Ganoti[83], C. Garabatos[106], E. Garcia-Solis[11], K. Garg[27], C. Gargiulo[33], A. Garibli[86], K. Garner[144], P. Gasik[104,117], E.F. Gauger[119], M.B. Gay Ducati[70], M. Germain[114], J. Ghosh[109], P. Ghosh[141], S.K. Ghosh[3], P. Gianotti[51], P. Giubellino[58,106], P. Giubilato[28], P. Glässel[103], D.M. Goméz Coral[71], A. Gomez Ramirez[74], V. Gonzalez[106], P. González-Zamora[44], S. Gorbunov[38], L. Görlich[118], S. Gotovac[34], V. Grabski[71], L.K. Graczykowski[142], K.L. Graham[110], L. Greiner[79], A. Grelli[63], C. Grigoras[33], V. Grigoriev[92], A. Grigoryan[1], S. Grigoryan[75], O.S. Groettvik[21], F. Grosa[30], J.F. Grosse-Oetringhaus[33], R. Grosso[106], R. Guernane[78], M. Guittiere[114], K. Gulbrandsen[88], T. Gunji[132], A. Gupta[100], R. Gupta[100], I.B. Guzman[44], R. Haake[146], M.K. Habib[106], C. Hadjidakis[61], H. Hamagaki[81], G. Hamar[145], M. Hamid[6], R. Hannigan[119], M.R. Haque[63,85], A. Harlenderova[106], J.W. Harris[146], A. Harton[11], J.A. Hasenbichler[33], H. Hassan[95], D. Hatzifotiadou[10,53], P. Hauer[42], S. Hayashi[132], S.T. Heckel[68,104], E. Hellbär[68], H. Helstrup[35], A. Herghelegiu[47], T. Herman[36], E.G. Hernandez[44], G. Herrera Corral[9], F. Herrmann[144], K.F. Hetland[35], T.E. Hilden[43], H. Hillemanns[33], C. Hills[127], B. Hippolyte[136], B. Hohlweger[104], D. Horak[36], A. Hornung[68], S. Hornung[106], R. Hosokawa[15,133], P. Hristov[33], C. Huang[61], C. Hughes[130], P. Huhn[68], T.J. Humanic[96], H. Hushnud[109], L.A. Husova[144], N. Hussain[41], S.A. Hussain[14], D. Hutter[38], J.P. Iddon[33,127], R. Ilkaev[108], M. Inaba[133], G.M. Innocenti[33], M. Ippolitov[87], A. Isakov[94], M.S. Islam[109], M. Ivanov[106], V. Ivanov[97], V. Izucheev[90], B. Jacak[79], N. Jacazio[53], P.M. Jacobs[79], S. Jadlovska[116], J. Jadlovsky[116], S. Jaelani[63], C. Jahnke[121], M.J. Jakubowska[142], M.A. Janik[142], T. Janson[74], M. Jercic[98], O. Jevons[110], M. Jin[125], F. Jonas[95,144], P.G. Jones[110], J. Jung[68], M. Jung[68], A. Jusko[110], P. Kalinak[64], A. Kalweit[33], V. Kaplin[92], S. Kar[6], A. Karasu Uysal[77], O. Karavichev[62], T. Karavicheva[62], P. Karczmarczyk[33], E. Karpechev[62], A. Kazantsev[87], U. Kebschull[74], R. Keidel[46], M. Keil[33], B. Ketzer[42], Z. Khabanova[89], A.M. Khan[6], S. Khan[16], S.A. Khan[141], A. Khanzadeev[97], Y. Kharlov[90], A. Khatun[16], A. Khuntia[118], B. Kileng[35], B. Kim[60], B. Kim[133], D. Kim[147], D.J. Kim[126], E.J. Kim[73], H. Kim[17,147], J. Kim[147], J.S. Kim[40], J. Kim[103], J. Kim[147], J. Kim[73], M. Kim[103], S. Kim[18], T. Kim[147], T. Kim[147], S. Kirsch[38,68], I. Kisel[38], S. Kiselev[91], A. Kisiel[142], J.L. Klay[5], C. Klein[68], J. Klein[58], S. Klein[79], C. Klein-Bösing[144], M. Kleiner[68], A. Kluge[33], M.L. Knichel[33], A.G. Knospe[125], C. Kobdaj[115], M.K. Köhler[103], T. Kollegger[106], A. Kondratyev[75], N. Kondratyeva[92], E. Kondratyuk[90], J. Konig[68], P.J. Konopka[33], L. Koska[116], O. Kovalenko[84], V. Kovalenko[112], M. Kowalski[118], I. Králik[64], A. Kravčáková[37], L. Kreis[106], M. Krivda[64,110], F. Krizek[94], K. Krizkova Gajdosova[36], M. Krüger[68], E. Kryshen[97], M. Krzewicki[38], A.M. Kubera[96], V. Kučera[60], C. Kuhn[136], P.G. Kuijer[89], L. Kumar[99], S. Kumar[48], S. Kundu[85], P. Kurashvili[84], A. Kurepin[62], A.B. Kurepin[62], A. Kuryakin[108], S. Kushpil[94], J. Kvapil[110], M.J. Kweon[60], J.Y. Kwon[60], Y. Kwon[147], S.L. La Pointe[38], P. La Rocca[27], Y.S. Lai[79], R. Langoy[129], K. Lapidus[33], A. Lardeux[20], P. Larionov[51], E. Laudi[33], R. Lavicka[36], T. Lazareva[112], R. Lea[24], L. Leardini[103], J. Lee[133], S. Lee[147], F. Lehas[89], S. Lehner[113], J. Lehrbach[38], R.C. Lemmon[93], I. León Monzón[120], E.D. Lesser[19], M. Lettrich[33], P. Lévai[145], X. Li[12], X.L. Li[6], J. Lien[129], R. Lietava[110], B. Lim[17], V. Lindenstruth[38], S.W. Lindsay[127], C. Lippmann[106], M.A. Lisa[96], V. Litichevskyi[43], A. Liu[19], S. Liu[96], W.J. Llope[143], I.M. Lofnes[21], V. Loginov[92], C. Loizides[95], P. Loncar[34], X. Lopez[134], E. López Torres[8], J.R. Luhder[144], M. Lunardon[28], G. Luparello[59], Y. Ma[39], A. Maevskaya[62], M. Mager[33], S.M. Mahmood[20], T. Mahmoud[42], A. Maire[136], R.D. Majka[146], M. Malaev[97], Q.W. Malik[20], L. Malinina[75,iii], D. Mal'Kevich[91], P. Malzacher[106], G. Mandaglio[55], V. Manko[87], F. Manso[134], V. Manzari[52], Y. Mao[6], M. Marchisone[135], J. Mareš[66], G.V. Margagliotti[24], A. Margotti[53], J. Margutti[63], A. Marín[106], C. Markert[119], M. Marquard[68], N.A. Martin[103], P. Martinengo[33], J.L. Martinez[125], M.I. Martínez[44], G. Martínez García[114], M. Martinez Pedreira[33], S. Masciocchi[106], M. Masera[25], A. Masoni[54], L. Massacrier[61], E. Masson[114], A. Mastroserio[52,138], A.M. Mathis[104,117], O. Matonoha[80], P.F.T. Matuoka[121], A. Matyja[118], C. Mayer[118], M. Mazzilli[52], M.A. Mazzoni[57], A.F. Mechler[68], F. Meddi[22], Y. Melikyan[62,92], A. Menchaca-Rocha[71], C. Mengke[6], E. Meninno[29,113], M. Meres[13], S. Mhlanga[124], Y. Miake[133], L. Micheletti[25], D.L. Mihaylov[104], K. Mikhaylov[75,91], A. Mischke[63,i],A.N. Mishra[69], D. Miśkowiec[106], A. Modak[3], N. Mohammadi[33], A.P. Mohanty[63], B. Mohanty[85], M. Mohisin Khan[16,iv], C. Mordasini[104], D.A. Moreira De Godoy[144], L.A.P. Moreno[44], I. Morozov[62], A. Morsch[33], T. Mrnjavac[33], V. Muccifora[51], E. Mudnic[34], D. Mühlheim[144], S. Muhuri[141], J.D. Mulligan[79], M.G. Munhoz[121], R.H. Munzer[68], H. Murakami[132], S. Murray[124], L. Musa[33], J. Musinsky[64], C.J. Myers[125], J.W. Myrcha[142], B. Naik[48], R. Nair[84], B.K. Nandi[48], R. Nania[10,53], E. Nappi[52], M.U. Naru[14], A.F. Nassirpour[80], C. Nattrass[130], R. Nayak[48], T.K. Nayak[85], S. Nazarenko[108], A. Neagu[20], R.A. Negrao De Oliveira[68], L. Nellen[69], S.V. Nesbo[35], G. Neskovic[38], D. Nesterov[112], L.T. Neumann[142], B.S. Nielsen[88], S. Nikolaev[87], S. Nikulin[87], V. Nikulin[97], F. Noferini[10,53], P. Nomokonov[75], J. Norman[78,127], N. Novitzky[133], P. Nowakowski[142], A. Nyanin[87], J. Nystrand[21], M. Ogino[81], A. Ohlson[80,103], J. Oleniacz[142], A.C. Oliveira Da Silva[121,130], M.H. Oliver[146], C. Oppedisano[58], R. Orava[43], A. Ortiz Velasquez[69], A. Oskarsson[80], J. Otwinowski[118], K. Oyama[81], Y. Pachmayer[103], V. Pacik[88], D. Pagano[140], G. Paić[69], J. Pan[143], A.K. Pandey[48], S. Panebianco[137], P. Pareek[49,141], J. Park[60], J.E. Parkkila[126], S. Parmar[99], S.P. Pathak[125], R.N. Patra[141], B. Paul[23,58], H. Pei[6], T. Peitzmann[63], X. Peng[6], L.G. Pereira[70], H. Pereira Da Costa[137], D. Peresunko[87], G.M. Perez[8], E. Perez Lezama[68], V. Peskov[68], Y. Pestov[4], V. Petráček[36], M. Petrovici[47], R.P. Pezzi[70], S. Piano[59], M. Pikna[13], P. Pillot[114], O. Pinazza[33,53], L. Pinsky[125], C. Pinto[27], S. Pisano[10,51], D. Pistone[55], M. Płoskoń[79], M. Planinic[98], F. Pliquett[68], J. Pluta[142], S. Pochybova[145,i],M.G. Poghosyan[95], B. Polichtchouk[90], N. Poljak[98], A. Pop[47], H. Poppenborg[144], S. Porteboeuf-Houssais[134], V. Pozdniakov[75], S.K. Prasad[3], R. Preghenella[53], F. Prino[58], C.A. Pruneau[143], I. Pshenichnov[62], M. Puccio[25,33], J. Putschke[143], R.E. Quishpe[125], S. Ragoni[110], S. Raha[3], S. Rajput[100], J. Rak[126], A. Rakotozafindrabe[137], L. Ramello[31], F. Rami[136], R. Raniwala[101], S. Raniwala[101], S.S. Räsänen[43], R. Rath[49], V. Ratza[42], I. Ravasenga[30,89], K.F. Read[95,130], K. Redlich[84,v],A. Rehman[21], P. Reichelt[68], F. Reidt[33], X. Ren[6], R. Renfordt[68], Z. Rescakova[37], J.-P. Revol[10], K. Reygers[103], V. Riabov[97], T. Richert[80,88], M. Richter[20], P. Riedler[33], W. Riegler[33], F. Riggi[27], C. Ristea[67], S.P. Rode[49], M. Rodríguez Cahuantzi[44], K. Røed[20], R. Rogalev[90], E. Rogochaya[75], D. Rohr[33], D. Röhrich[21], P.S. Rokita[142], F. Ronchetti[51], E.D. Rosas[69], K. Roslon[142], A. Rossi[28,56], A. Rotondi[139], A. Roy[49], P. Roy[109], O.V. Rueda[80], R. Rui[24], B. Rumyantsev[75], A. Rustamov[86], E. Ryabinkin[87], Y. Ryabov[97], A. Rybicki[118], H. Rytkonen[126], O.A.M. Saarimaki[43], S. Sadhu[141], S. Sadovsky[90], K. Šafařík[36], S.K. Saha[141], B. Sahoo[48], P. Sahoo[48,49], R. Sahoo[49], S. Sahoo[65], P.K. Sahu[65], J. Saini[141], S. Sakai[133], S. Sambyal[100], V. Samsonov[92,97], D. Sarkar[143], N. Sarkar[141], P. Sarma[41], V.M. Sarti[104], M.H.P. Sas[63], E. Scapparone[53], B. Schaefer[95], J. Schambach[119], H.S. Scheid[68], C. Schiaua[47], R. Schicker[103], A. Schmah[103], C. Schmidt[106], H.R. Schmidt[102], M.O. Schmidt[103], M. Schmidt[102], N.V. Schmidt[68,95], A.R. Schmier[130], J. Schukraft[88], Y. Schutz[33,136], K. Schwarz[106], K. Schweda[106], G. Scioli[26], E. Scomparin[58], M. Šefčík[37], J.E. Seger[15], Y. Sekiguchi[132], D. Sekihata[132], I. Selyuzhenkov[92,106], S. Senyukov[136], D. Serebryakov[62], E. Serradilla[71], A. Sevcenco[67], A. Shabanov[62], A. Shabetai[114], R. Shahoyan[33], W. Shaikh[109], A. Shangaraev[90], A. Sharma[99], A. Sharma[100], H. Sharma[118], M. Sharma[100], N. Sharma[99], A.I. Sheikh[141], K. Shigaki[45], M. Shimomura[82], S. Shirinkin[91], Q. Shou[39], Y. Sibiriak[87], S. Siddhanta[54], T. Siemiarczuk[84], D. Silvermyr[80], G. Simatovic[89], G. Simonetti[33,104], R. Singh[85], R. Singh[100], R. Singh[49], V.K. Singh[141], V. Singhal[141], T. Sinha[109], B. Sitar[13], M. Sitta[31], T.B. Skaali[20], M. Slupecki[126], N. Smirnov[146], R.J.M. Snellings[63], T.W. Snellman[43,126], C. Soncco[111], J. Song[60,125], A. Songmoolnak[115], F. Soramel[28], S. Sorensen[130], I. Sputowska[118], J. Stachel[103], I. Stan[67], P. Stankus[95], P.J. Steffanic[130], E. Stenlund[80], D. Stocco[114], M.M. Storetvedt[35], L.D. Stritto[29], A.A.P. Suaide[121], T. Sugitate[45], C. Suire[61], M. Suleymanov[14],

M. Suljic[33], R. Sultanov[91], M. Šumbera[94], S. Sumowidagdo[50], S. Swain[65], A. Szabo[13], I. Szarka[13], U. Tabassam[14], G. Taillepied[134], J. Takahashi[122], G.J. Tambave[21], S. Tang[6,134], M. Tarhini[114], M.G. Tarzila[47], A. Tauro[33], G. Tejeda Muñoz[44], A. Telesca[33], C. Terrevoli[125], D. Thakur[49], S. Thakur[141], D. Thomas[119], F. Thoresen[88], R. Tieulent[135], A. Tikhonov[62], A.R. Timmins[125], A. Toia[68], N. Topilskaya[62], M. Toppi[51], F. Torales-Acosta[19], S.R. Torres[9,120], A. Trifiro[55], S. Tripathy[49], T. Tripathy[48], S. Trogolo[28], G. Trombetta[32], L. Tropp[37], V. Trubnikov[2], W.H. Trzaska[126], T.P. Trzcinski[142], B.A. Trzeciak[63], T. Tsuji[132], A. Tumkin[108], R. Turrisi[56], T.S. Tveter[20], K. Ullaland[21], E.N. Umaka[125], A. Uras[135], G.L. Usai[23], A. Utrobicic[98], M. Vala[37], N. Valle[139], S. Vallero[58], N. van der Kolk[63], L.V.R. van Doremalen[63], M. van Leeuwen[63], P. Vande Vyvre[33], D. Varga[145], Z. Varga[145], M. Varga-Kofarago[145], A. Vargas[44], M. Vasileiou[83], A. Vasiliev[87], O. Vázquez Doce[104,117], V. Vechernin[112], A.M. Veen[63], E. Vercellin[25], S. Vergara Limón[44], L. Vermunt[63], R. Vernet[7], R. Vértesi[145], L. Vickovic[34], Z. Vilakazi[131], O. Villalobos Baillie[110], A. Villatoro Tello[44], G. Vino[52], A. Vinogradov[87], T. Virgili[29], V. Vislavicius[88], A. Vodopyanov[75], B. Volkel[33], M.A. Völkl[102], K. Voloshin[91], S.A. Voloshin[143], G. Volpe[32], B. von Haller[33], I. Vorobyev[104], D. Voscek[116], J. Vrláková[37], B. Wagner[21], M. Weber[113], S.G. Weber[144], A. Wegrzynek[33], D.F. Weiser[103], S.C. Wenzel[33], J.P. Wessels[144], J. Wiechula[68], J. Wikne[20], G. Wilk[84], J. Wilkinson[10,53], G.A. Willems[33], E. Willsher[110], B. Windelband[103], M. Winn[137], W.E. Witt[130], Y. Wu[128], R. Xu[6], S. Yalcin[77], K. Yamakawa[45], S. Yang[21], S. Yano[137], Z. Yin[6], H. Yokoyama[63], I.-K. Yoo[17], J.H. Yoon[60], S. Yuan[21], A. Yuncu[103], V. Yurchenko[2], V. Zaccolo[24], A. Zaman[14], C. Zampolli[33], H.J.C. Zanoli[63], N. Zardoshti[33], A. Zarochentsev[112], P. Závada[66], N. Zaviyalov[108], H. Zbroszczyk[142], M. Zhalov[97], S. Zhang[39], X. Zhang[6], Z. Zhang[6], V. Zherebchevskii[112], D. Zhou[6], Y. Zhou[88], Z. Zhou[21], J. Zhu[6,106], Y. Zhu[6], A. Zichichi[10,26], M.B. Zimmermann[33], G. Zinovjev[2], N. Zurlo[140]

[1] *A.I. Alikhanyan National Science Laboratory (Yerevan Physics Institute) Foundation, Yerevan, Armenia*
[2] *Bogolyubov Institute for Theoretical Physics, National Academy of Sciences of Ukraine, Kiev, Ukraine*
[3] *Bose Institute, Department of Physics and Centre for Astroparticle Physics and Space Science (CAPSS), Kolkata, India*
[4] *Budker Institute for Nuclear Physics, Novosibirsk, Russia*
[5] *California Polytechnic State University, San Luis Obispo, CA, United States*
[6] *Central China Normal University, Wuhan, China*
[7] *Centre de Calcul de l'IN2P3, Villeurbanne, Lyon, France*
[8] *Centro de Aplicaciones Tecnológicas y Desarrollo Nuclear (CEADEN), Havana, Cuba*
[9] *Centro de Investigación y de Estudios Avanzados (CINVESTAV), Mexico City and Mérida, Mexico*
[10] *Centro Fermi – Museo Storico della Fisica e Centro Studi e Ricerche "Enrico Fermi', Rome, Italy*
[11] *Chicago State University, Chicago, IL, United States*
[12] *China Institute of Atomic Energy, Beijing, China*
[13] *Comenius University Bratislava, Faculty of Mathematics, Physics and Informatics, Bratislava, Slovakia*
[14] *COMSATS University Islamabad, Islamabad, Pakistan*
[15] *Creighton University, Omaha, NE, United States*
[16] *Department of Physics, Aligarh Muslim University, Aligarh, India*
[17] *Department of Physics, Pusan National University, Pusan, Republic of Korea*
[18] *Department of Physics, Sejong University, Seoul, Republic of Korea*
[19] *Department of Physics, University of California, Berkeley, CA, United States*
[20] *Department of Physics, University of Oslo, Oslo, Norway*
[21] *Department of Physics and Technology, University of Bergen, Bergen, Norway*
[22] *Dipartimento di Fisica dell'Università 'La Sapienza' and Sezione INFN, Rome, Italy*
[23] *Dipartimento di Fisica dell'Università and Sezione INFN, Cagliari, Italy*
[24] *Dipartimento di Fisica dell'Università and Sezione INFN, Trieste, Italy*
[25] *Dipartimento di Fisica dell'Università and Sezione INFN, Turin, Italy*
[26] *Dipartimento di Fisica e Astronomia dell'Università and Sezione INFN, Bologna, Italy*
[27] *Dipartimento di Fisica e Astronomia dell'Università and Sezione INFN, Catania, Italy*
[28] *Dipartimento di Fisica e Astronomia dell'Università and Sezione INFN, Padova, Italy*
[29] *Dipartimento di Fisica 'E.R. Caianiello' dell'Università and Gruppo Collegato INFN, Salerno, Italy*
[30] *Dipartimento DISAT del Politecnico and Sezione INFN, Turin, Italy*
[31] *Dipartimento di Scienze e Innovazione Tecnologica dell'Università del Piemonte Orientale and INFN Sezione di Torino, Alessandria, Italy*
[32] *Dipartimento Interateneo di Fisica 'M. Merlin' and Sezione INFN, Bari, Italy*
[33] *European Organization for Nuclear Research (CERN), Geneva, Switzerland*
[34] *Faculty of Electrical Engineering, Mechanical Engineering and Naval Architecture, University of Split, Split, Croatia*
[35] *Faculty of Engineering and Science, Western Norway University of Applied Sciences, Bergen, Norway*
[36] *Faculty of Nuclear Sciences and Physical Engineering, Czech Technical University in Prague, Prague, Czech Republic*
[37] *Faculty of Science, P.J. Šafárik University, Košice, Slovakia*
[38] *Frankfurt Institute for Advanced Studies, Johann Wolfgang Goethe-Universität Frankfurt, Frankfurt, Germany*
[39] *Fudan University, Shanghai, China*
[40] *Gangneung-Wonju National University, Gangneung, Republic of Korea*
[41] *Gauhati University, Department of Physics, Guwahati, India*
[42] *Helmholtz-Institut für Strahlen- und Kernphysik, Rheinische Friedrich-Wilhelms-Universität Bonn, Bonn, Germany*
[43] *Helsinki Institute of Physics (HIP), Helsinki, Finland*
[44] *High Energy Physics Group, Universidad Autónoma de Puebla, Puebla, Mexico*
[45] *Hiroshima University, Hiroshima, Japan*
[46] *Hochschule Worms, Zentrum für Technologietransfer und Telekommunikation (ZTT), Worms, Germany*

[47] *Horia Hulubei National Institute of Physics and Nuclear Engineering, Bucharest, Romania*
[48] *Indian Institute of Technology Bombay (IIT), Mumbai, India*
[49] *Indian Institute of Technology Indore, Indore, India*
[50] *Indonesian Institute of Sciences, Jakarta, Indonesia*
[51] *INFN, Laboratori Nazionali di Frascati, Frascati, Italy*
[52] *INFN, Sezione di Bari, Bari, Italy*
[53] *INFN, Sezione di Bologna, Bologna, Italy*
[54] *INFN, Sezione di Cagliari, Cagliari, Italy*
[55] *INFN, Sezione di Catania, Catania, Italy*
[56] *INFN, Sezione di Padova, Padova, Italy*
[57] *INFN, Sezione di Roma, Rome, Italy*
[58] *INFN, Sezione di Torino, Turin, Italy*
[59] *INFN, Sezione di Trieste, Trieste, Italy*
[60] *Inha University, Incheon, Republic of Korea*
[61] *Institut de Physique Nucléaire d’Orsay (IPNO), Institut National de Physique Nucléaire et de Physique des Particules (IN2P3/CNRS), Université de Paris-Sud, Université Paris-Saclay, Orsay, France*
[62] *Institute for Nuclear Research, Academy of Sciences, Moscow, Russia*
[63] *Institute for Subatomic Physics, Utrecht University/Nikhef, Utrecht, Netherlands*
[64] *Institute of Experimental Physics, Slovak Academy of Sciences, Košice, Slovakia*
[65] *Institute of Physics, Homi Bhabha National Institute, Bhubaneswar, India*
[66] *Institute of Physics of the Czech Academy of Sciences, Prague, Czech Republic*
[67] *Institute of Space Science (ISS), Bucharest, Romania*
[68] *Institut für Kernphysik, Johann Wolfgang Goethe-Universität Frankfurt, Frankfurt, Germany*
[69] *Instituto de Ciencias Nucleares, Universidad Nacional Autónoma de México, Mexico City, Mexico*
[70] *Instituto de Física, Universidade Federal do Rio Grande do Sul (UFRGS), Porto Alegre, Brazil*
[71] *Instituto de Física, Universidad Nacional Autónoma de México, Mexico City, Mexico*
[72] *iThemba LABS, National Research Foundation, Somerset West, South Africa*
[73] *Jeonbuk National University, Jeonju, Republic of Korea*
[74] *Johann-Wolfgang-Goethe Universität Frankfurt Institut für Informatik, Fachbereich Informatik und Mathematik, Frankfurt, Germany*
[75] *Joint Institute for Nuclear Research (JINR), Dubna, Russia*
[76] *Korea Institute of Science and Technology Information, Daejeon, Republic of Korea*
[77] *KTO Karatay University, Konya, Turkey*
[78] *Laboratoire de Physique Subatomique et de Cosmologie, Université Grenoble-Alpes, CNRS-IN2P3, Grenoble, France*
[79] *Lawrence Berkeley National Laboratory, Berkeley, CA, United States*
[80] *Lund University Department of Physics, Division of Particle Physics, Lund, Sweden*
[81] *Nagasaki Institute of Applied Science, Nagasaki, Japan*
[82] *Nara Women’s University (NWU), Nara, Japan*
[83] *National and Kapodistrian University of Athens, School of Science, Department of Physics, Athens, Greece*
[84] *National Centre for Nuclear Research, Warsaw, Poland*
[85] *National Institute of Science Education and Research, Homi Bhabha National Institute, Jatni, India*
[86] *National Nuclear Research Center, Baku, Azerbaijan*
[87] *National Research Centre Kurchatov Institute, Moscow, Russia*
[88] *Niels Bohr Institute, University of Copenhagen, Copenhagen, Denmark*
[89] *Nikhef, National institute for subatomic physics, Amsterdam, Netherlands*
[90] *NRC Kurchatov Institute IHEP, Protvino, Russia*
[91] *NRC «Kurchatov Institute»– ITEP, Moscow, Russia*
[92] *NRNU Moscow Engineering Physics Institute, Moscow, Russia*
[93] *Nuclear Physics Group, STFC Daresbury Laboratory, Daresbury, United Kingdom*
[94] *Nuclear Physics Institute of the Czech Academy of Sciences, Řež u Prahy, Czech Republic*
[95] *Oak Ridge National Laboratory, Oak Ridge, TN, United States*
[96] *Ohio State University, Columbus, OH, United States*
[97] *Petersburg Nuclear Physics Institute, Gatchina, Russia*
[98] *Physics department, Faculty of science, University of Zagreb, Zagreb, Croatia*
[99] *Physics Department, Panjab University, Chandigarh, India*
[100] *Physics Department, University of Jammu, Jammu, India*
[101] *Physics Department, University of Rajasthan, Jaipur, India*
[102] *Physikalisches Institut, Eberhard-Karls-Universität Tübingen, Tübingen, Germany*
[103] *Physikalisches Institut, Ruprecht-Karls-Universität Heidelberg, Heidelberg, Germany*
[104] *Physik Department, Technische Universität München, Munich, Germany*
[105] *Politecnico di Bari, Bari, Italy*
[106] *Research Division and ExtreMe Matter Institute EMMI, GSI Helmholtzzentrum für Schwerionenforschung GmbH, Darmstadt, Germany*
[107] *Rudjer Bošković Institute, Zagreb, Croatia*
[108] *Russian Federal Nuclear Center (VNIIEF), Sarov, Russia*
[109] *Saha Institute of Nuclear Physics, Homi Bhabha National Institute, Kolkata, India*
[110] *School of Physics and Astronomy, University of Birmingham, Birmingham, United Kingdom*
[111] *Sección Física, Departamento de Ciencias, Pontificia Universidad Católica del Perú, Lima, Peru*
[112] *St. Petersburg State University, St. Petersburg, Russia*
[113] *Stefan Meyer Institut für Subatomare Physik (SMI), Vienna, Austria*
[114] *SUBATECH, IMT Atlantique, Université de Nantes, CNRS-IN2P3, Nantes, France*
[115] *Suranaree University of Technology, Nakhon Ratchasima, Thailand*
[116] *Technical University of Košice, Košice, Slovakia*
[117] *Technische Universität München, Excellence Cluster ‘Universe’, Munich, Germany*
[118] *The Henryk Niewodniczanski Institute of Nuclear Physics, Polish Academy of Sciences, Cracow, Poland*
[119] *The University of Texas at Austin, Austin, TX, United States*
[120] *Universidad Autónoma de Sinaloa, Culiacán, Mexico*
[121] *Universidade de São Paulo (USP), São Paulo, Brazil*
[122] *Universidade Estadual de Campinas (UNICAMP), Campinas, Brazil*
[123] *Universidade Federal do ABC, Santo Andre, Brazil*
[124] *University of Cape Town, Cape Town, South Africa*
[125] *University of Houston, Houston, TX, United States*

[126] *University of Jyväskylä, Jyväskylä, Finland*
[127] *University of Liverpool, Liverpool, United Kingdom*
[128] *University of Science and Technology of China, Hefei, China*
[129] *University of South-Eastern Norway, Tonsberg, Norway*
[130] *University of Tennessee, Knoxville, TN, United States*
[131] *University of the Witwatersrand, Johannesburg, South Africa*
[132] *University of Tokyo, Tokyo, Japan*
[133] *University of Tsukuba, Tsukuba, Japan*
[134] *Université Clermont Auvergne, CNRS/IN2P3, LPC, Clermont-Ferrand, France*
[135] *Université de Lyon, Université Lyon 1, CNRS/IN2P3, IPN-Lyon, Villeurbanne, Lyon, France*
[136] *Université de Strasbourg, CNRS, IPHC UMR 7178, F-67000 Strasbourg, France*
[137] *Université Paris-Saclay Centre d'Etudes de Saclay (CEA), IRFU, Départment de Physique Nucléaire (DPhN), Saclay, France*
[138] *Università degli Studi di Foggia, Foggia, Italy*
[139] *Università degli Studi di Pavia, Pavia, Italy*
[140] *Università di Brescia, Brescia, Italy*
[141] *Variable Energy Cyclotron Centre, Homi Bhabha National Institute, Kolkata, India*
[142] *Warsaw University of Technology, Warsaw, Poland*
[143] *Wayne State University, Detroit, MI, United States*
[144] *Westfälische Wilhelms-Universität Münster, Institut für Kernphysik, Münster, Germany*
[145] *Wigner Research Centre for Physics, Budapest, Hungary*
[146] *Yale University, New Haven, CT, United States*
[147] *Yonsei University, Seoul, Republic of Korea*

[i] Deceased.
[ii] Dipartimento DET del Politecnico di Torino, Turin, Italy.
[iii] M.V. Lomonosov Moscow State University, D.V. Skobeltsyn Institute of Nuclear, Physics, Moscow, Russia.
[iv] Department of Applied Physics, Aligarh Muslim University, Aligarh, India.
[v] Institute of Theoretical Physics, University of Wroclaw, Poland.